Title
Correlated Phases of Weyl Semi-Metals

Author
Wei, Huazhou

Publication Date
2013

Peer reviewed|Thesis/dissertation

UNIVERSITY OF CALIFORNIA
RIVERSIDE

Correlated Phases of Weyl Semi-Metals

A Dissertation submitted in partial satisfaction
of the requirements for the degree of

Doctor of Philosophy

in

Physics

by

Huazhou Wei

August 2013

Dissertation Committee:

Professor Vivek Aji, Chairperson
Professor Chandra Varma
Professor Shan-Wen Tsai

The Dissertation of Huazhou Wei is approved:

Committee Chairperson

University of California, Riverside

Acknowledgments

Firstly, I would like to express my deepest and the most sincere gratitude to my Ph.D. advisor, Professor Vivek Aji. He is passionate in research and has always been encouraging me to be involved in the fascinating problem of the appearance of novel phases in Weyl Semi-Metals, almost since the first day I joined his research group. During the past several years, his profound physics insight provided me with great guidance in the course of my Ph.D. research.

The most sincere thanks from me, are also due to the other two committee members, Prof. Chandra Varma and Prof. Shan-Wen Tsai, for their endless help they have provided to me during my whole Ph.D. studies, especially their introduction of me to my Ph.D. advisor, Prof. Vivek Aji, which makes me really grateful to both of them indeed.

Throughout my Ph.D. work, I made a lot of collaborations and had many useful discussions with Sung-Po Chao, a former member in Dr. Aji's research group. He taught me plenty of mathematica techniques and analytical methods. I wish to extend my warmest thanks to him as well. Also I wish him best of luck and great success in the future.

I am greatly indebted to my wife, Xiaojuan Tian, who has made enormous contribution to our family and continuous effort in powering me up to be always positive while facing any difficulty or frustration, which always plays the role of driving force in my heart during my Ph.D. studies. Meanwhile I want to express my deepest grateful to my parents, Zhongyang Wei and Liming Zhou, and my two elder sisters, Li Wei, and Dongyun Wei. I want to thank my parents for bringing me to the world and their love and care from childhood. I also want to thank my sisters for their love and support these years. Their love and support have always been very well received.

In the end, I'd like to say 'Thank you' to Univ. of California, Riverside, for their Dean's Distinguished Fellowship Award, and Department of Physics & Astronomy in Univ. of California, Riverside, for their kindly offer during my application seasons.

To my parents & my wife

ABSTRACT OF THE DISSERTATION

Correlated Phases of Weyl Semi-Metals

by

Huazhou Wei

Doctor of Philosophy, Graduate Program in Physics
University of California, Riverside, August 2013
Professor Vivek Aji, Chairperson

Weyl Semi-Metals are materials whose properties are strongly influenced by spin-orbit couplings. Their description, at low energies, is in terms of non-relativistic linearly dispersing massless fermions. In this thesis, we explore possible of new correlated phases. In particular we focus on excitonic phases due to particle-hole instabilities in chapters 2, and 3, and on superconducting phases from particle-particle instabilities in chapter 4.

The range of the interaction plays a crucial role in determining the most stable phase. For particle-hole instabilities, short-range interactions yield eight phases. At stoichiometry, they all require minimum interaction strengths to ensure their emergence. Only one of them, the chiral excitonic insulator(EI) phase, opens a gap at the nodes. It is energetically most favored and is characterized by a complex vectorial order parameter. Also, it is ferromagnetic with the phase of the order parameter determining the direction of the induced net spin polarization's. In contrast long-range interactions can condense a second gapped state namely the Charge Density Wave (CDW). To highlight the physics, we employ the multipole expansion and analyze to leading order. Expanding the interaction potential ($\propto 1/|\vec{k}-\vec{k'}|$) and the order parameter $\Delta(\vec{k})$ in spherical harmonics, the gap equation is

obtained and analyzed to obtain the minimum interaction strengths linked to phases. We end that the critical coupling for CDW phase is half that of the EI phase. Thus, under the Coulomb interaction, CDW phase is more energetically favorable.

In chapter 4, we turn to possible superconducting states induced by particle-particle instabilities. As the energy spectrum has even nodes in the Brillouin zone, both intra-nodal finite-momentum pairing and inter-nodal zero-momentum BCS pairing are allowed. For local attractive interaction the finite momentum pairing state with chiral p-wave symmetry is the most favorable phase at finite carrier density. For chemical potential at the node the state is preempted by a fully gapped CDW phase. On the other hand, for long-range attractive interactions, the p-wave BCS superconducting state wins out for all values of the chemical potential.

Contents

List of Figures

Chapter 1

Introduction

1.1 What is a Weyl Semi-Metal?

The emergence of materials whose properties are strongly influenced by spin orbit coupling is an exciting new phenomenon in condensed matter physics. A prototypical example of this type of materials is the topological insulator[5, 6], which has garnered much attention[7, 8, 9]. Another canonical example of this type of materials is the one that we focus on in this thesis: Weyl Semi-Metals[3, 4, 10, 11, 12]. The low energy description in these systems is in terms of Weyl fermions. We will start our introduction by reviewing the knowledge of Dirac fermions and carry out the transition to Weyl fermions and Weyl Semi-Metals step by step in the following several sections.

1.1.1 Dirac Fermions

Low-dimensional materials are among of the most actively researched systems in condensed matter physics. The most well-known examples are graphene[13, 14] and topological insulators[15, 16]. These are often termed Dirac materials because of the emergence

of Dirac fermions in their low energy description[17, 18, 19]. In the vicinity of Fermi energy, the excitations are described by the Dirac Equation:

$$\big(-i\vec{\alpha}\cdot\vec{\nabla}+\beta m\big)\psi = i\frac{\partial\psi}{\partial t} \tag{1.1}$$

where ψ is the four-component Dirac spinor, and α, β are the 4×4 Dirac gamma matrices:

$$\vec{\alpha} = \begin{bmatrix} \mathbf{0} & \vec{\sigma} \\ \vec{\sigma} & \mathbf{0} \end{bmatrix}; \beta = \begin{bmatrix} \mathbf{I} & \mathbf{0} \\ \mathbf{0} & -\mathbf{I} \end{bmatrix} \tag{1.2}$$

$\mathbf{0}$ and $\mathbf{I}$ are 2×2 matrices. In order to get the plane wave solutions, we write the four-component Dirac spinor ψ as:

$$\psi(\vec{r},t) = u(\vec{p})e^{-i(Et-\vec{p}\cdot\vec{r})} = \begin{pmatrix} \chi \\ \phi \end{pmatrix} e^{-i(Et-\vec{p}\cdot\vec{r})} \tag{1.3}$$

Here, $u(\vec{p})$ is a four-component spinor, and both χ and ϕ are two-component spinors. So the Dirac equation becomes:

$$\begin{pmatrix} m & \vec{\sigma}\cdot\vec{p} \\ \vec{\sigma}\cdot\vec{p} & -m \end{pmatrix} \begin{pmatrix} \chi \\ \phi \end{pmatrix} = E \begin{pmatrix} \chi \\ \phi \end{pmatrix} \tag{1.4}$$

Here, we have dropped the exponential factors. The general solution of above equation is:

$$\begin{aligned} \chi &= \frac{\vec{\sigma}\cdot\vec{p}}{E-m}\phi \\ \phi &= \frac{\vec{\sigma}\cdot\vec{p}}{E+m}\chi \end{aligned} \tag{1.5}$$

These are solutions to the Dirac equation provided the energy eigenvalues take the form:

$$E^2 = |\vec{p}|^2 + m^2 \tag{1.6}$$

For massless fermions, the energy dispersion a linear function of momentum[17, 18, 19]. This is indeed the case in graphene for energies close to the node as seen in Fig.(1.1)[1]. The same is also true for the surface states of three dimensional topological insulators[20, 21, 6, 8, 7].

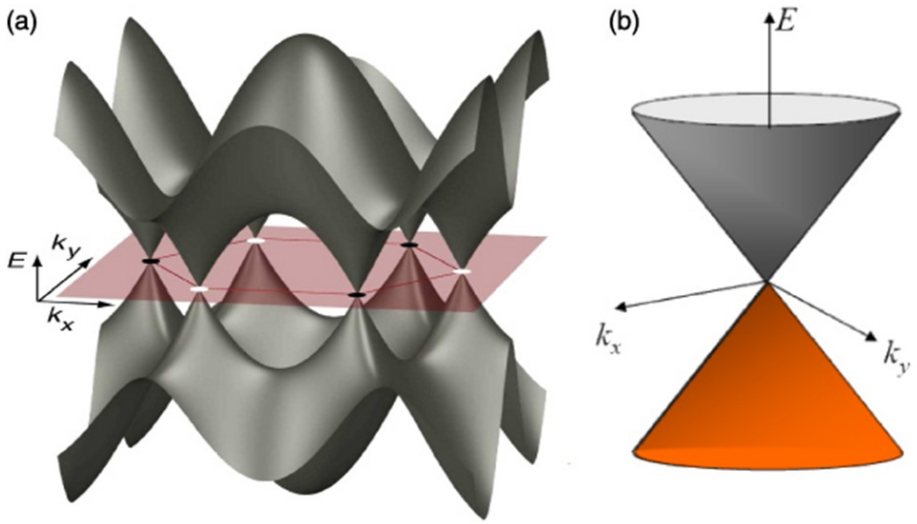

Figure 1.1: Band structure of two-dimensional graphene layer, where the hexagonal first Brillouin zone is indicated. This graph is reproduced from C. W. J. Beenakker's review article: Refs.[1].

While the mass goes to zero, the Dirac equation reads:

$$\begin{pmatrix} 0 & \vec{\sigma}\cdot\vec{p} \\ \vec{\sigma}\cdot\vec{p} & 0 \end{pmatrix} \begin{pmatrix} \chi \\ \phi \end{pmatrix} = E \begin{pmatrix} \chi \\ \phi \end{pmatrix} \tag{1.7}$$

which results in:

$$\begin{aligned} \left(\vec{\sigma}\cdot\vec{p}\right)\chi &= E\phi \\ \left(\vec{\sigma}\cdot\vec{p}\right)\phi &= E\chi \end{aligned} \tag{1.8}$$

The above relations imply thatχ and ϕ are not independent with each other. However, a linear combination between χ and ϕ in the following form:

$$\begin{aligned} \Psi_R &= \frac{1}{2}(\chi+\phi) \\ \Psi_L &= \frac{1}{2}(\chi-\phi) \end{aligned} \tag{1.9}$$

yields:

$$
\begin{aligned}
+\left(\vec{\sigma}\cdot\vec{p}\right)\Psi_R &= E\Psi_R \\
-\left(\vec{\sigma}\cdot\vec{p}\right)\Psi_L &= E\Psi_L
\end{aligned}
\tag{1.10}
$$

The two redefined two-component spinors, Ψ_R and Ψ_L are called Weyl spinors. They are decoupled from each other and are considered independent particles. They are characterized by a conserved quantum number called chirality[22]. Eigenstates of the operator $\vec{\sigma}\cdot\vec{p}/|\vec{p}|$, chirality is the projection of angular momentum $\vec{\sigma}$ on the momentum $\hat{p}$. For angular momentum parallel to linear momentum, the chirality is + while for antiparallel alignment it is −. For massless particles this quantum number is conserved. Fig.(1.2) depicts the two possibilities.

1.1.2 Weyl Fermions

The 'Weyl equation' has its origin in high energy physics[23, 24]. It was introduced by German physicist Hermann Weyl[25] as a relativistic wave equation for describing massless spin-1/2 particles. While Dirac equations, albeit in two dimensions, have been the focus of condensed matter physicist over the last decade, Weyl fermions have gained prominence over the past couple of years. They add to the growing list of topologically nontrivial phenomena possible in the solid state.

Being described by two-component wave functions as opposed to the four-component Dirac spinors, Weyl fermions occur in systems where two non-degenerate bands meet with each other at limited number of isolated points in the Brillouin zone. In general the existence of such Weyl nodes at the chemical potential is accidental[26], but if they do exist, they are robust against perturbations that are translationally invariant.

The linear dependence of energy on momentum is reminiscent of studies in rela-

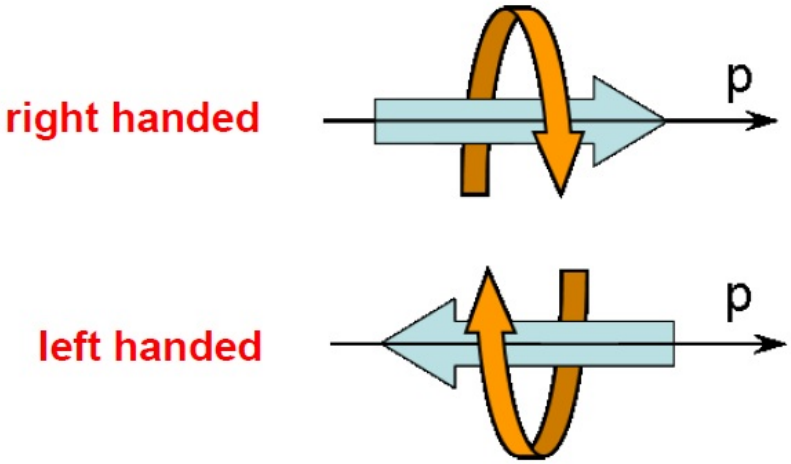

Figure 1.2: Relation of angular momentum's direction and momentum for particles with +1 chirality (upper case) and −1 chirality (lower case). This graph is taken from D. J. Miller's presentation[2] in SUPA graduate school in 2008.

tivistic high energy physics. The chemical potential is at the node and as such much of the phenomena studied is of interest to a wider community beyond condensed matter physicists. The spectrum in the low energy limit of Weyl Semi-Metal systems can be regarded as three dimensional graphene-like materials. However, there are still considerable differences between Weyl Semi-Metal systems and other linear dispersing energy spectrum materials, such as graphene, whose band structure is displayed in Fig.(1.1)[1].

An important property of Weyl Semi-Metal systems is that the systems are robust to most translationally-invariant interactions. This is exactly a consequence of chirality being a conserved quantum number in three dimensions for massless fermions, while for two dimensions it is not a conserved quantum number. As a result of this restriction coming from the chirality conservation for linear dispersing massless fermions in three dimensions, therefore only those interactions which could couple different fermions with opposite chirality can open a uniform gap at the Weyl nodes in Weyl Semi-Metal systems.

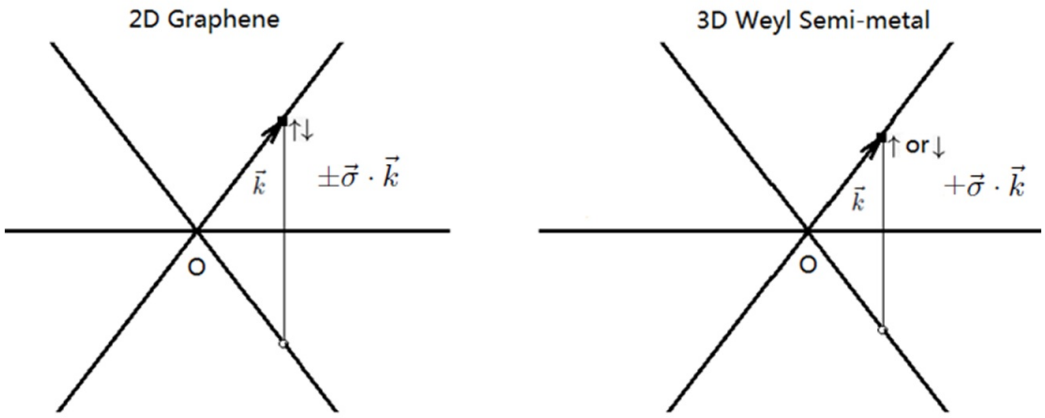

Figure 1.3: Band structure comparison between 2D graphene and 3D Weyl Semi-Metal system. Detailed degeneracy properties in both cases are indicated explicitly. In order to highlight the key point, we only plot one linearly node in each chase, however, in the Weyl systems, Weyl nodes always appear in pairs with opposite chiralities.

Another difference between Weyl Semi-Metals systems and graphene systems, is the degeneracy of the energy spectrums. Inversion symmetry and time-reversal symmetry are preserved in graphene ensuring the two-fold spin degeneracy in graphene's two dimensional energy spectrum. However, in contrast, in the three dimensional Weyl Semi-Metal systems, either inversion symmetry or time-reversal symmetry is broken. Thus the non-degeneracy property of their energy spectra. The comparison is shown in Fig.(1.3). The non-degeneracy property of Weyl Semi-Metal's band structure originates from the strong spin-orbit coupling in Weyl systems. The spin orientation is either $\vec{\sigma}$ parallel to $\vec{k}$ or $\vec{\sigma}$ antiparallel to $\vec{k}$, which is determined by the sign of chirality in each node ($+1$ or -1). Thus in Weyl Semi-Metal systems that preserve inversion symmetry but break time reversal symmetry, each Weyl node in the momentum space, is accompanied by another Weyl node with opposite chirality in the Brillouin zone. Thus there are even number of nodes

mandated by symmetry.

1.1.3 Possible Realization of Weyl Semi-Metals

While the physics of Weyl fermions has been extensively studied in the context of liquid ^{3}He[27, 28] where they arise in the A phase, the developments of study for Weyl fermions in condensed matter context has just started [3, 4, 10, 11, 12, 29, 30, 31, 32, 33]. These works have renewed interest in Weyl Semi-Metal systems and their possible realization in nature. Weyl fermions are conjectured to be the low energy excitations of two type of possible Weyl Semi-Metal structures: Pyrochlore Irradiates[3, 34, 35] and Topological-Normal Insulator heterostructures[4]. In these materials, the semi-metallic nature is preserved by the touching of two non-degenerate bands at even numbers of Weyl points in the vicinity of or at the chemical potential. The conservation of chirality at each node implies that only interactions that couple nodes can open gaps. As such these systems provide an interesting new platform to study the interplay of interaction and spin orbit in establishing new states of matter.

The first possible realization of Weyl Semi-Metals[3] is in Pyrochlore Iridates. On each hexagonal zone boundary there are three Weyl points. Thus 24 Weyl points are expected in Pyrochlore Iridates structures[3]. Please refer to the three-dimensional Brillouin zone of $Y_2Ir_2O_7$ in Fig.(1.4). For each pair of Weyl nodes with opposite chiralities, there is perfect nest in. Refs.[3] focused on the pyrochlore iridates, which have the general formula $A_2Ir_2O_7$, where A=yttrium or a lanthanide element. In the pyrochlore iridates, both A and Ir atoms are located on a network of corner-sharing tetrahedra[36, 37, 38]. Data from experiments indicate the existence of magnetic order for $A_2Ir_2O_7$[39], which breaks the time-reversal symmetry. Other experiments[40] revealed an evolution of ground-state properties

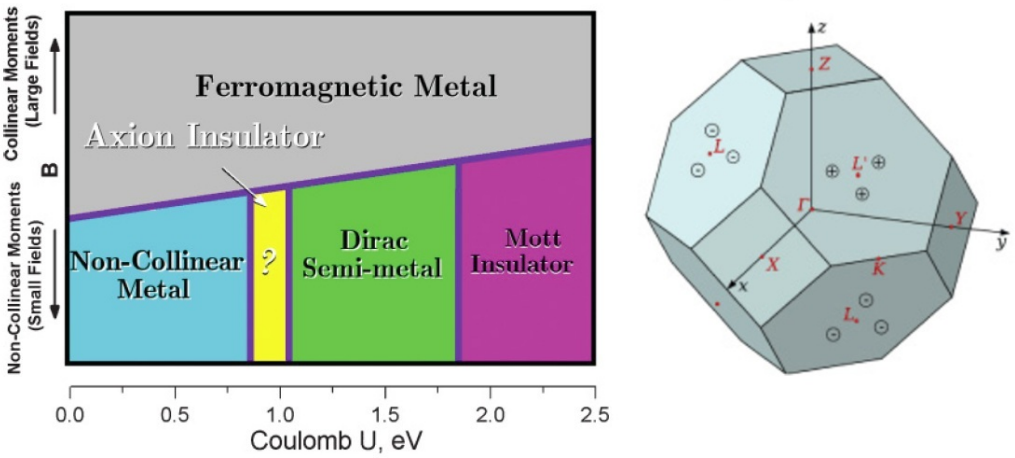

Figure 1.4: left: Sketch of the predicted phase diagram for Pyrochlore Iridates: horizontal axis is the increasing interaction among Ir 5d electrons; vertical axis is the external magnetic field, which can trigger a transition out of the noncollinear all-in/all-out ground state, which has several electronic phases. right:Three-dimensional Brillouin zone of $Y_2Ir_2O_7$ (one example of Pyrochlore Iridates), where locations of the Weyl points are depicted (nine are shown, indicated by the circled + or − signs). The source of the two graphs is: Refs.[3].

with increasing radius of the A ion, which is believed to tune electron correlations. While A = Pr is metallic, A = Y is an insulator at low temperatures. Those data are explained by authors in Refs.[3], where the electronic structure calculations confirm the evolution and give a novel ground state. The magnetic moments order on Ir sites in a noncollinear pattern, with moment on a tetrahedron pointing all in or all out from the center. The structure preserves inversion symmetry and the electronic properties evolve with correlation strength. For weak correlations, or in the absence of magnetic order, a metal is obtained; while with strong correlations, a Mott insulator with all-in/all-out magnetic order is found. And for the case between the two limits with intermediate correlations, the electronic ground state is found to be a Weyl Semi-Metal, with linearly dispersing nodes at the chemical potential. In this phase time-reversal symmetry is broken and inversion symmetry is preserved.

The second possible realization of a Weyl Semi-Metal system[4] is in the superlattice heterostructures, which is made of alternating layers of topological insulator and normal insulator, which is shown in Fig.(1.5). In Refs.[4] the topological-normal insulator heterostructures proposed is the simplest realization of the three-dimensional Weyl Semi-Metal phase with only two Weyl nodes carrying opposite chirality separated in momentum space. This is achieved by utilizing a multilayer structure composed of identical thin films of a magnetically doped three-dimensional topological insulator layers, separated by ordinary-insulator spacer layers. The doped magnetic impurities in Topological Insulator layers leads to spin splitting of the surface states. This is the source of time-reversal breaking in the Weyl System, as the magnetic impurities ferromagnetically order with magnetization along the growth direction of the heterostructures.

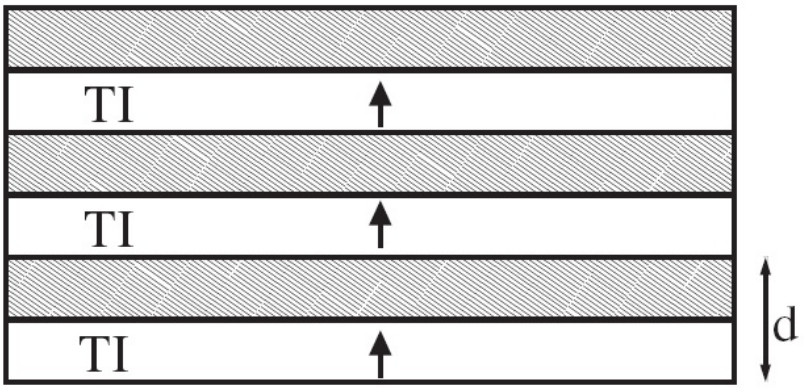

Figure 1.5: Schematic drawing of the three-dimensional multilayer heterostructures obtained by alternating Topological Insulator(TI) layers and Normal Insulator(NI) layers, where for all of the TI layers, their surface states' time-reversal symmetry is broken caused by doping magnetic impurities inside TI layers. Unhashed layers are the TI layers, while hashed layers are the NI spacers. The arrow in each TI layer shows the magnetization direction. Only three periods of the superlattice are shown in the schematic. This graph originates from Refs.[4].

1.2 Our Interests in Weyl Semi-Metals

In Weyl Semi-Metals, various phenomenon originate due to the low-energy effective theory being in terms of massless linearly dispersing fermions in three dimensions. As a new topological state of matter, Weyl Semi-Metal is characterized by the presence of non-degenerate band-touching nodes, separated by Fermi level in its band structure in momentum space. In Weyl systems, the robust protection of the semi-metallic physics against translationally invariant perturbations is a consequence of chirality being a good quantum number. The origin of the phenomena can be traced back to the existence of strong spin-orbit coupling. this in turn can compete with other interactions and energy scale seeding the idea that Weyl Semi-Metals systems should be an ideal place to explore new correlated novel phases of matter. This is the motivation of my research and my

interests are mainly focused on the emergence of new phases of matter in Weyl Semi-Metal Systems.

In this thesis, I will show that the interplay between general density-density interaction and topology can promote various novel phases, including excitonic phases[41] yielded by particle-hole instability and superconducting phases originating from particle-particle instability. In each case, we seek novel phases in two limits: short-range limit(momentum-independent interaction) and long-range limit(Coulomb form interaction); and for each limit, the interaction terms can be divided into two types: inter-nodal part and intra-nodal part. The results for excitonic phases yielded by particle-hole instability are described in chapter 2 and chapter 3, while the results for superconducting phases originating from particle-particle instability is described in chapter 4. It is worth noting that the interactions we considered in the following three chapters are repulsive, and the work on attractive interaction case is done by other scientists[30], which was obtained by them around the same time while we focused on our research under repulsive interaction. For the completeness of research on this topic, we include their results in the appendix.

Chapter 2

Excitonic Phases by Short-range Repulsive Interaction

In this chapter we focus on the appearance and properties of Charge Density Wave and Excitonic Insulating states in Weyl semi-metal systems. Particle hole pairs gain binding energy due to repulsive Coulomb interaction. Since we have two nodes, these pairs can have zero or finite momentum, Condensation of the former leads to excitonic insulators while the latter yield CDWs. The nature of these instabilities depends crucially on the range of interaction. As such we will compare the possible phases for short-range and long-range interactions.

2.1 Model Hamiltonian

In order to simplify the problem and highlight the physics, we consider a system with only two Weyl nodes, located at $\vec{K}_1 = K_0\hat{x}$ (labeled R) and $-\vec{K}_1 = -K_0\hat{x}$ (labeled L)

with their chiralities $+1$ and -1 respectively. The model hamiltonian reads:

$$H_{0\pm} = \pm\hbar v \sum_{\vec{k}} \psi^{\dagger}_{\vec{k}\alpha} \vec{\sigma}_{\alpha\beta} \cdot \left(\vec{k} \mp \vec{K}_0\right) \psi_{\vec{k}\beta} \tag{2.1}$$

where v is the fermi velocity and $\vec{\sigma} = \{\sigma_x, \sigma_y, \sigma_z\}$ is the vector of Pauli matrices. The linear energy dispersion relation at each node can be written in this form: $\epsilon_{\vec{q}} = \pm\hbar v \left|\vec{q}\right|$, both of which are centered around $\pm\vec{K}_0$ respectively, with $\vec{q} = \vec{k} \mp \vec{K}_0$. The Fermi levels located at the positions of the two Weyl nodes, The conduction (or valence) band at the R node has its spin parallel (or anti-parallel) to the reciprocal vector $\vec{q}$, while the opposite is true at the L node.

The general spin independent particle-particle interaction takes the form in the following:

$$\begin{aligned} V &= \sum_{\sigma,\sigma'} \int d\vec{r} d\vec{r}' V\left(\vec{r} - \vec{r}'\right) \psi^{\dagger}_{\sigma'}\left(\vec{r}'\right) \psi_{\sigma'}\left(\vec{r}'\right) \psi^{\dagger}_{\sigma}\left(\vec{r}\right) \psi_{\sigma}\left(\vec{r}\right) \\ &= \sum_{\sigma,\sigma'} \sum_{\vec{k},\vec{k}',\vec{q}} V(\vec{q}) \psi^{\dagger}_{\vec{k}'+\vec{q},\sigma'} \psi_{\vec{k}',\sigma'} \psi^{\dagger}_{\vec{k}-\vec{q},\sigma} \psi_{\vec{k},\sigma} \end{aligned} \tag{2.2}$$

Here $V(\vec{q}) = \frac{1}{\Omega} \int d\vec{r} V(\vec{r})$ with Ω being the volume of the Weyl semi-metal system that we considered in our model.

For the moment, we haven't made any assumptions on the nature of the interactions. Since the Weyl physics is the low energy description of a more general theory, we enforce an upper cutoff in the momentum integrals (up to $\left|\vec{q}\right| = \Lambda/\hbar v$ with a cutoff energy Λ) around each Weyl point. We first use mean field approach to study the various excitonic phases associated with different type of particle-hole interaction. Next we employ Ginzburg-Landau free energy expansions to obtain the nature of instability near the transition temperature as well as to obtain the condensation energies as a function of coupling constant for various phases. This will help establish the ground state for these materials.

2.2 Particle-Hole Instabilities within Mean Field

Let's begin by rewriting the interaction potential in the basis of the non-interacting bands. Define $\psi^{R,L}_{\vec{q},\pm} = \eta^{R,L}_{\vec{q},\pm} c^{R,L}_{\vec{q},\pm}$ as the fermionic fields of the conduction bands and valence bands, where η is the spinor and c is the fermion annihilation operator. Restricting to the low energy sector, only 6 of the 16 possible terms from Eq.(2.2) satisfy momentum conservation.

In order to simplify the expression of the general particle-particle interaction, we choose a new set of orthogonal coordinate system in the momentum space as below: $\hat{q} = \{\hat{q}_x, \hat{q}_y, \hat{q}_z\}$ which is the unit vector along $\vec{q}$, and another two vectors $\hat{e}^1_{\vec{q}} \equiv \hat{\theta}_{\vec{q}} = \{\hat{q}_x\hat{q}_z/\sqrt{\hat{q}_x^2+\hat{q}_y^2}, \hat{q}_y\hat{q}_z/\sqrt{\hat{q}_x^2+\hat{q}_y^2}, -\sqrt{\hat{q}_x^2+\hat{q}_y^2}\}$ and $\hat{e}^2_{\vec{q}} \equiv \hat{\phi}_{\vec{q}} = \{-\hat{q}_y/\sqrt{\hat{q}_x^2+\hat{q}_y^2}, \hat{q}_x/\sqrt{\hat{q}_x^2+\hat{q}_y^2}, 0\}$. It is worth noting that the new set of orthogonal coordinate system: $\hat{q}$, $\hat{e}^1_{\vec{q}}$ and $\hat{e}^2_{\vec{q}}$ is a right-handed coordinate system (please refer to Fig.2.1). The unit sphere is spanned by the vector $\hat{q}$ by two rotations, one about any axis perpendicular to $\hat{e}^2_{\vec{q}}$ and the another about $\hat{e}^2_{\vec{q}}$. For example if we choose the first to be the z-axis, than the vector $\hat{e}^2_{\vec{q}}$, which is the $\hat{\phi}$ in the spherical polar system, spans a unit circle (perimeter of the shaded region in Fig.2.1) and the vector $\vec{e}^1_{\vec{q}}$, which is the corresponding $\hat{\theta}$, spans the southern hemisphere. The following construction holds for an arbitrary quantization axis $\hat{n}$, with the corresponding polar and azimuthal angle for $\vec{q}$ defined in the coordinate frame $\{\hat{l}, \hat{m}, \hat{n}\}$.

Focusing on even function of momentum, $\vec{k}$, i.e. $V(\vec{k}) = V(-\vec{k})$, the interaction

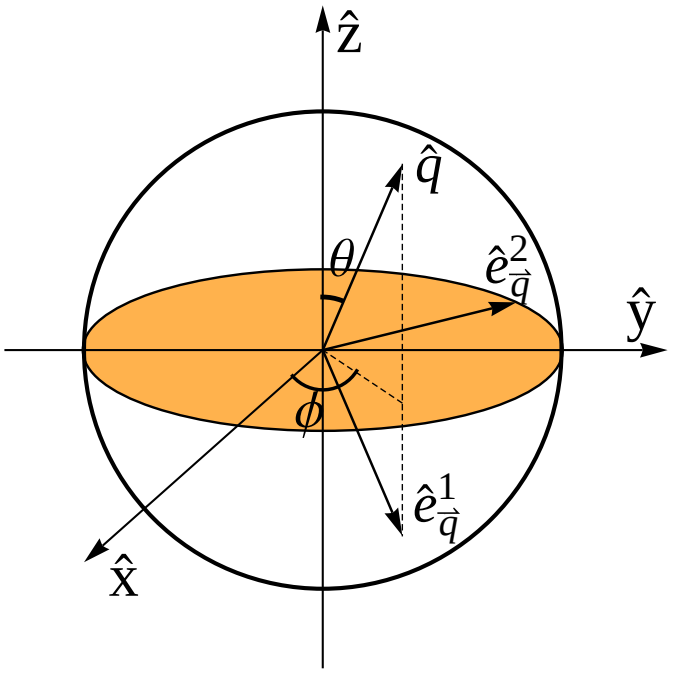

Figure 2.1: The interaction shown in Eq.(2.3) is a function of three vectors ($\hat{q}$, $\hat{e}^1_{\vec{q}}$ and $\hat{e}^2_{\vec{q}}$) that form a right handed coordinate system. Each vector couples to an operator of distinct symmetry in the particle hole channel.

simplifies $\hat{e}_{\vec{k}} = \hat{e}^1_{\vec{k}} + \imath \hat{e}^2_{\vec{k}}$,

$$\begin{aligned} V = -\sum_{\vec{k},\vec{k}',n=\pm} \Bigg[& V(\vec{k}-\vec{k}') \frac{\hat{e}_{\vec{k}} \cdot \hat{e}^*_{\vec{k}'} + \hat{e}^*_{\vec{k}} \cdot \hat{e}_{\vec{k}'}}{4} \sum_{\tau=R,L} c^{\tau\dagger}_{\vec{k},n} c^{\tau}_{\vec{k},-n} c^{\tau\dagger}_{\vec{k}',-n} c^{\tau}_{\vec{k}',n} \\ & + V(\vec{k}-\vec{k}'-2\vec{K}_0) \frac{\hat{e}_{\vec{k}} \cdot \hat{e}_{\vec{k}'} + \hat{e}^*_{\vec{k}} \cdot \hat{e}^*_{\vec{k}'}}{2} c^{L\dagger}_{\vec{k},n} c^{L}_{\vec{k},-n} c^{R\dagger}_{\vec{k}',-n} c^{R}_{\vec{k}',n} \\ & - \Big[2V(2\vec{K}_0) - V(\vec{k}-\vec{k}') \Big(\hat{k} \cdot \hat{k}' + 1 \Big) \Big] c^{L\dagger}_{\vec{k},n} c^{R}_{\vec{k},-n} c^{R\dagger}_{\vec{k}',-n} c^{L}_{\vec{k}',n} \Bigg] \end{aligned} \tag{2.3}$$

Here we have only considered the lowest energy channels involving the particle-hole instability. The effects of including all terms, which does not change the discussion in the main text, are discussed in Appendix A. The first and second term in the above Eq.(2.3) promote the Excitonic Insulator instabilities with intra-nodal order parameter, i.e. $\left\langle \sum_{\vec{k}} \vec{A}_{\vec{k}} c^{\tau\dagger}_{\vec{k},n} c^{\tau}_{\vec{k},-n} \right\rangle \neq 0$ where $\vec{A}_{\vec{k}}$ is an odd function of $\vec{k}$; while the last term in the above Eq.(2.3) leads to the Charge Density Wave instabilities described by the inter-nodal

order parameter with $\left\langle \sum_{\vec{k}} \vec{A}_{\vec{k}} c^{\tau\dagger}_{\vec{k},n} c^{\bar{\tau}}_{\vec{k},-n} \right\rangle \neq 0$.

In the rest of this section, we will analyze all the possible symmetry broken states. These are dictated by the fact that:

1. $\vec{A}_{\vec{k}}$ is one of three possible vectors $\{\hat{q},\, \hat{e}^1_{\vec{q}},\, \hat{e}^2_{\vec{q}}\}$;

2. rotational invariance is broken;

3. the state is either polar or chiral in nature.

These lead to eight possible novel particle-hole instabilities promoted by the presence of short-range repulsive interaction. A summary of the main results can be found in table 2.1.

2.3 Inter-nodal Charge Density Wave

We begin by studying the inter-nodal instability that establishes ordering at $2\vec{K}_0$ (third term in Eq.(2.3)).Fpr short ranged repulsion the interaction is $V(\vec{k}) = g/\Omega$, where $g > 0$ is the repulsive interaction strength. Under this assumption, the coupling term, third one in Eq.(2.3), takes the following form:

$$V_{eff} = -\frac{g}{\Omega} \sum_{\vec{k},\vec{k}'} \sum_{n=\pm} \left(\hat{k} c^{L\dagger}_{\vec{k},n} c^{R}_{\vec{k},-n} \right) \cdot \left(\hat{k}' c^{R\dagger}_{\vec{k}',-n} c^{L}_{\vec{k}',n} \right) \tag{2.4}$$

$\vec{A}_{\hat{k}}$	State	$\left\langle \vec{A}_k \right\rangle \propto$	Spectrum	g_c
$\hat{k}$	Chiral	$\hat{x} + i\hat{y}$	Gapless	3
	Polar	$\hat{z}$	Gapless	3
$\hat{e}^1_{\vec{k}}$	Chiral-z	$\hat{x} + i\hat{y}$	Gapless	6
	Polar-z	$\hat{z}$	Gapless	3
	Polar-x	$\hat{x}$	Gapless	12
	Chiral-x	$\hat{y} + i\hat{z}$	Gapless	4.8
$\hat{e}^2_{\vec{k}}$	Polar	$\hat{x}$	Gapless	4
	Chiral	$\hat{x} + i\hat{y}$	Gapped	2

Table 2.1: Possible excitonic phases, their symmetries, whether they gap out the Weyl node or not and the critical coupling in units of $(\hbar v)^3 / 2\pi\Lambda^2$.

Eq.(2.4) is identical to that of the interaction in ^{3}He in the particle-particle channel that leads to chiral superfluidity[27, 28]. Similarly in Weyl semi-metals case, the corresponding state in the particle-hole channel is proven to be a charge density wave state. Within mean field[28][42], there would be two possible particle-hole instabilities:

1. Chiral CDW: $\vec{\Delta}_c = \frac{g}{\Omega}\left\langle \sum_{\vec{k'}} \hat{k'} c^{\tau\dagger}_{\vec{k'},n} c^{\bar{\tau}}_{\vec{k'},-n} \right\rangle = \Delta_c(\frac{\hat{x}+\imath\hat{y}}{\sqrt{2}})$
2. Polar CDW: $\vec{\Delta}_p = \frac{g}{\Omega}\left\langle \sum_{\vec{k'}} \hat{k'} c^{\tau\dagger}_{\vec{k'},n} c^{\bar{\tau}}_{\vec{k'},-n} \right\rangle = \Delta_p \hat{z}$

Note that the directions chosen for the ground state is for convenience and all other possibilities which can be obtained by coordinate system rotation in three dimensions are equivalent. The first one is a chiral state while the second one is a non-chiral p wave Charge Density Wave state. Combining the effective inter-nodal repulsive interaction in Eq.(2.4) with the model hamiltonian in Eq.(2.1), we are get the mean-field Hamiltonian for the interacting Weyl semimetal system :

$$H_{MF} = \sum_{\vec{q},n} \begin{pmatrix} c^L_{\vec{q},n} \\ \\ c^R_{\vec{q},-n} \end{pmatrix}^\dagger \begin{pmatrix} \hbar v n|\vec{q}| & -\vec{\Delta}\cdot\hat{q} \\ \\ -\vec{\Delta}^*\cdot\hat{q} & -\hbar v n|\vec{q}| \end{pmatrix} \begin{pmatrix} c^L_{\vec{q},n} \\ \\ c^R_{\vec{q},-n} \end{pmatrix} \tag{2.5}$$

Here, $\vec{\Delta}$ representing $\vec{\Delta}_c$ or $\vec{\Delta}_p$ is the vectorial order parameter of the system. Following the standard mean field procedure, we diagonalize this Hamiltonian by applying a Bogoliubov transformation[28] and minimize the system's free energy with respect to the vectorial order parameter's magnitude $|\vec{\Delta}\cdot\hat{q}|$. The self-consistent integral equation which determines the interaction strength and leads to the particle-hole instability takes the form:

$$1 = \frac{g}{\Omega}\sum_{\vec{k}} \frac{|\hat{\Delta}_{c/p}\cdot\hat{k}|^2}{2E_{\vec{k}}} \tanh\frac{\beta E_{\vec{k}}}{2} \tag{2.6}$$

Here $E_{\vec{k}} = \sqrt{(\hbar v|\vec{k}|)^2 + |\vec{\Delta}\cdot\hat{k}|^2}$, and $\beta = 1/k_BT$. Also $\hat{\Delta}_{c/p}$ represents the unit vector direction of chiral or polar state, and $\Omega = \frac{8\pi}{3n}\left(\frac{\Lambda}{\hbar v}\right)^3$, where n is the number of electrons in

the system, which is set to 1 in the following calculation. The summation over momentum space has an upper cutoff with the scale $\Lambda/\hbar v$.

In the limit of $\Delta \ll \Lambda$ and zero temperature, we can expand the particle-hole instabilities gap equation Eq.(2.6) to the leading order with respect to the order parameter $\Delta_{c/p}$, which gives:

$$\begin{aligned} 1 &\simeq \frac{\pi g \Lambda^2}{(\hbar v)^3}\left[\frac{2}{3} + \left(\frac{-17 - 30\ln 2}{225} + \frac{4\ln\left(\frac{\Delta_c}{2\Lambda}\right)}{15}\right)\frac{\Delta_c^2}{\Lambda^2} + \dots\right] \\ 1 &\simeq \frac{\pi g \Lambda^2}{(\hbar v)^3}\left[\frac{2}{3} + \left(\frac{3}{25} + \frac{2}{5}\ln\left(\frac{\Delta_p}{2\Lambda}\right)\right)\frac{\Delta_p^2}{\Lambda^2} + \dots\right] \end{aligned} \tag{2.7}$$

Both of the two possible instabilities share the same critical value for the coupling constant. Now we can see: for $g > 3(\hbar v)^3/2\pi\Lambda^2$ there exists charge density wave instability within mean field approach. Crucially the charge density wave instability does not gap out the Weyl nodes, therefore the conduction bands and valence bands still meet at the two nodes and there are no non-zero gap opened.

We further analyze the instability by studying the gap as a function of coupling strength using Eq.(2.6). For every interaction strength g, we can calculate the corresponding order parameter magnitude Δ from Eq.(2.6). After normalizing the quantities to be dimensionless, we plot the result in Fig.2.2. From the plot, we can see the two particle-hole instabilities states indeed share the same instability threshold, just like the results we achieved through analytically expansion. Also, the magnitude of the order parameter is larger for the chiral state, as compared to the polar state for the same interaction strength.

We can analyze the phase transition further by looking at the condensation energy and how it changes as we modify the interaction magnitude. Here, the condensation energy, denoted as E_c, is defined as the zero temperature free energy difference between the condensate charge density wave states and the normal states. By taking the similar procedure like

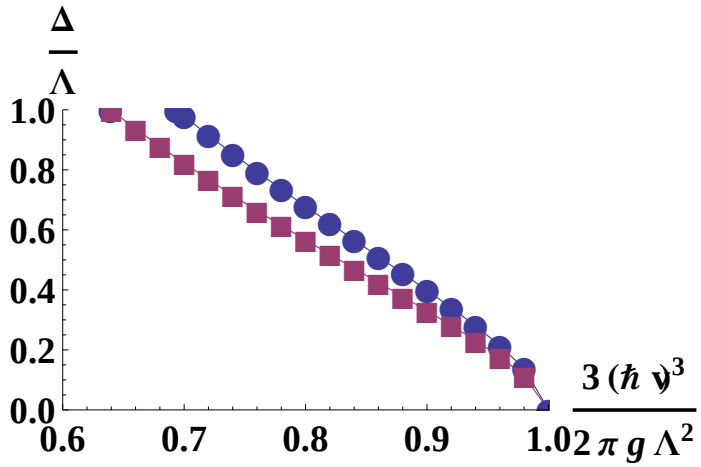

Figure 2.2: Gap magnitude of the two charge density wave states. Order parameter magnitude as a function of inverse of the interaction strength for chiral (blue ○) and polar (purple □) states.

above, for every interaction strength g, we calculate the corresponding condensation energy E_c by getting the difference of zero temperature free energy between charge density wave condensation states and normal states. After dimensionless normalization the results are shown in Fig.2.3, where the magnitude of the condensation energy of the two charge density wave states are plotted as a function of the interaction strength. From the plot, we see that the chiral state yields a greater (more negative) condensation energy, compared with the polar state at the same interaction magnitude. Therefore in this sector the lowest energy state is the chiral charge density state which can be regarded as the new ground state of the Weyl semimetal system at the presence of inter-nodal repulsive short-range interaction.

2.4 Ginzburg-Landau Free Energy Analysis

To study the temperature dependence we employ the Ginzburg Landau theory[43] for a single order. For chemical potential near the Weyl node, the free energy related to the

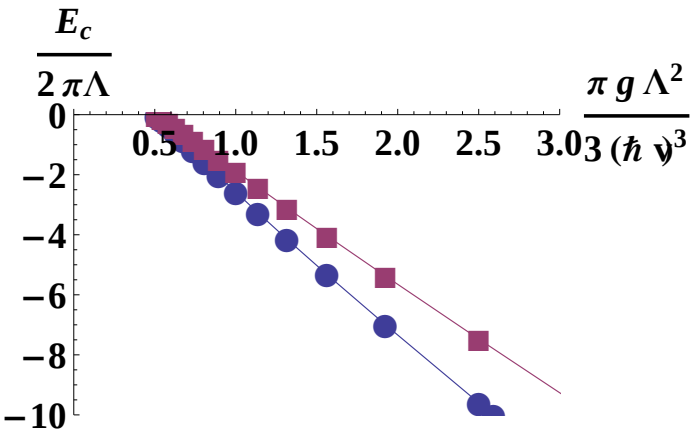

Figure 2.3: Condensation energy of the two charge density wave states. Condensation energy E_c with $\mu = 0$ for chiral (blue $\circ$) and polar (purple $\square$) states as a function of the interaction strength.

charge density wave state's order parameter is:

$$\begin{aligned} F_{CDW} &= \sum_{\vec{q},\alpha} E_{\vec{q}\alpha} f(E_{\vec{q},\alpha}) - \sum_{\vec{q},\alpha} \left(E_{\vec{q},\alpha} - \hbar v_F |\vec{q_\alpha}| - \frac{|\vec{\Delta}\cdot\hat{q}|^2}{g} \right) - TS \\ &= \sum_{\vec{q},\alpha} E_{\vec{q},\alpha} f(E_{\vec{q},\alpha}) + 2E_c - TS \end{aligned} \tag{2.8}$$

Here the entropy S take the general form:

$$S = -k_B \sum_{\vec{q},\alpha} \left[\Big(1 - f(E_{\vec{q},\alpha})\Big) \ln \Big(1 - f(E_{\vec{q},\alpha})\Big) + f(E_{\vec{q},\alpha}) \ln f(E_{\vec{q},\alpha}) \right] \tag{2.9}$$

And $\alpha = L, R$, denotes the indices for the quasi particles obtained by the Bogoliubov transformation[28]. $E_c \equiv -\frac{1}{2}\sum_{\vec{q},\alpha} \left(E_{\vec{q},\alpha} - \hbar v_F |\vec{q_\alpha}| - \frac{|\vec{\Delta}\cdot\hat{q}|^2}{g} \right)$ is the condensate (exciton pairs) energy. We can rewrite Eq.(2.8) to be:

$$\begin{aligned} F_{CDW} &= -\frac{1}{\beta} \ln Tr(e^{-\beta \hat{H}}) \\ &= -\frac{1}{\beta} \sum_{\vec{q},\alpha} \ln \left(1 + e^{-\beta E_{\vec{q},\alpha}} \right) + 2E_c \end{aligned} \tag{2.10}$$

Here, considering the known free energy expression of normal Fermi liquid state:

$$F_N = -\frac{1}{\beta} \sum_{\vec{q},\alpha} \ln \left(1 + e^{-\beta \hbar v q_\alpha} \right) \tag{2.11}$$

We can find that the free energy difference between charge density wave state and the normal Fermi liquid state is:

$$\begin{aligned} F_{CDW} - F_N &= F_{CDW} + \frac{1}{\beta}\sum_{\vec{q},\alpha} \ln\left(1 + e^{-\beta\hbar v q_\alpha}\right) \\ &= -\frac{1}{\beta}\sum_{\vec{q},\alpha} \ln\frac{1+e^{-\beta E_{q\vec{\alpha}}}}{1+e^{-\beta\hbar v q_\alpha}} - \sum_{\vec{q},\alpha}\left(E_{\vec{q},\alpha} - \hbar v_F|\vec{q_\alpha}| - \frac{|\vec{\Delta}\cdot\hat{q}|^2}{g}\right) \end{aligned} \tag{2.12}$$

For $T \simeq T_c$, both $F_{CN} \equiv F_{CDW} - F_N \to 0$ and $\Delta_0(T) \to 0$. Hence we can express the condensation energy F_{CN} as a functional of $|\vec{\Delta}_{c/p}(T)\cdot\hat{q}| = A^{\hat{q}}_{c/p}\Delta_{c/p}(T)$ for the chiral $\left(A^{\hat{q}}_c = \hat{\Delta}_c\cdot\hat{q} = \frac{|\hat{q}_x|\pm i|\hat{q}_y|}{\sqrt{2}}\right)$ or polar $\left(A^{\hat{q}}_p = |\hat{q}_z|\right)$ charge density wave phases and expand the partial derivative of F_{CN} in the Taylor series as:

$$\begin{aligned} \frac{1}{\Delta_{c/p}}\frac{\partial F_{CN}}{\partial\Delta^*_{c/p}} &= -\frac{1}{2\Delta_{c/p}}\sum_{\vec{q},\alpha}\left\{\left[1-2f(E_{\vec{q_\alpha}})\right]\frac{\partial E_{\vec{q_\alpha}}}{\partial\Delta^*_{c/p}} - \frac{|A^{\hat{q}}_{c/p}|^2\Delta_{c/p}}{g}\right\} \\ &= -\sum_{\vec{q}}\frac{|A^{\hat{q}}_{c/p}|^2}{2}\left\{\frac{1}{E_{\vec{q}}}\tanh\frac{\beta E_{\vec{q}}}{2} - \frac{1}{\epsilon_{\vec{q}}}\tanh\frac{\beta_c\epsilon_{\vec{q}}}{2}\right\} \\ &\simeq \sum_{\vec{q}}|A^{\hat{q}}_{c/p}|^2\left[\frac{f(\beta\epsilon_{\vec{q}}) - f(\beta_c\epsilon_{\vec{q}})}{\epsilon_{\vec{q}}} + \sum_{n=-\infty}^{\infty}\frac{\beta_c^3|\Delta_{c/p}|^2|A^{\hat{q}}_{c/p}|^2}{((2n+1)^2\pi^2+\beta_c^2\epsilon^2_{\vec{q}})^2} + O(|\Delta_{c/p}|^4) + \dots\right] \end{aligned} \tag{2.13}$$

Because for $T \simeq T_c$ the free energy difference has the general following form:

$$F_{CN} = -a_{c/p}|\Delta_{c/p}|^2 + \frac{b_{c/p}}{2}|\Delta_{c/p}|^4 + \dots \tag{2.14}$$

Therefore for the chiral charge density wave phase, the coefficients of the above free energy difference expression are:

$$\begin{aligned} a_c = a_p &\simeq \frac{4\pi}{3k_BT}\left(\frac{1}{\beta_c\hbar v}\right)^3\left(1-\frac{T}{T_c}\right) \\ b_c = \frac{2}{3}b_p &= \frac{8\pi}{15(\hbar v)^3}\sum_{n=0}^{\infty}\left[\frac{\frac{\pi(2n+1)}{\beta_c\Lambda}}{\frac{\pi^2(2n+1)^2}{\beta_c^2\Lambda^2}+1} + \frac{\tan^{-1}\left(\frac{\beta_c\Lambda}{\pi(2n+1)}\right)}{\pi(2n+1)}\right] \\ &\simeq \frac{8\pi}{15(\hbar v)^3}\left[\frac{\beta_c\Lambda}{2}\ln 2 + \frac{1}{4}\ln\left(\frac{\beta_c\Lambda}{2\pi}\right) - \frac{1}{4}\Psi\left(\frac{1}{2}\right)\right] \end{aligned} \tag{2.15}$$

The coefficient a_c in the above Eq.(2.15) is to leading order in $(\beta_c\Lambda)^{-1}$ and $\Psi(x)$ is the digamma function. The critical temperature T_c, evaluated by taking $\Delta \to 0$ at $T = T_c$ in Eq.(2.6), is $k_B T_c \simeq \sqrt{\frac{3}{\pi^2}(\Lambda^2 - \frac{3(\hbar v)^3}{2\pi g})}$. For the polar charge density wave phase, the coefficient a_p is the same as a_c and b_p is $\frac{3}{2}b_c$. Thus the critical temperature T_c in polar charge density wave phase, is the same as that in the chiral charge density wave phase. On the other hand, the coefficient of the quartic term is smaller for the chiral phase and hence it has the larger order parameter magnitude and even lower free energies comparing with polar phase. Therefore, we conclude that the most stable state in the inter-nodal sector is the chiral charge density wave phase.

2.5 Intra-nodal Excitonic Insulator

Having established the particle-hole instabilities in the inter-nodal sector we turn to those promoted by the first two terms in Eq.(2.3). Focussing on momentum independent interaction: $V(\vec{q}) = \frac{g}{\Omega}$. we get:

$$V = -\frac{g}{2\Omega}\sum_{\vec{k},\vec{k}'}\left(\vec{\Phi}^{1*}_{\vec{k}}\cdot\vec{\Phi}^{1}_{\vec{k}'} + \vec{\Phi}^{2*}_{\vec{k}}\cdot\vec{\Phi}^{2}_{\vec{k}'}\right) \tag{2.16}$$

To make the symmetry content manifest we have rewritten the interaction in terms of operators $\Psi^1_{\vec{k}}$ and $\Psi^2_{\vec{k}}$. They are $\vec{\Phi}^1_{\vec{k}}$, and the part containing $\hat{e}^2_{\vec{k}}$ by another new symbol $\vec{\Phi}^2_{\vec{k}}$. Their definitions are:

$$\begin{aligned}\vec{\Phi}^1_{\vec{k}} &= \hat{e}^1_{\vec{k}}\left(c^{L\dagger}_{\vec{k},+}c^{L}_{\vec{k},-} + c^{R\dagger}_{\vec{k},+}c^{R}_{\vec{k},-}\right)\\ \vec{\Phi}^2_{\vec{k}} &= \hat{e}^2_{\vec{k}}\left(c^{L\dagger}_{\vec{k},+}c^{L}_{\vec{k},-} - c^{R\dagger}_{\vec{k},+}c^{R}_{\vec{k},-}\right)\end{aligned} \tag{2.17}$$

Let's first consider the order parameters related to the $\hat{e}^1_{\vec{k}}$ component. In the above expression, we can see that only the first term inside the summation $\vec{\Phi}^{1*}_{\vec{k}}\cdot\vec{\Phi}^{1}_{\vec{k}'}$ concerns the $\hat{e}^1_{\vec{k}}$

component. Hence together with the model hamiltonian Eq.(2.1), we find that there would be four possible particle-hole instabilities for order parameters related to $\hat{e}^1_{\vec{k}}$ component:

1. Chiral-z EI: $\vec{\Delta}^L_{cz1} + \vec{\Delta}^R_{cz1} = \frac{g}{2\Omega}\langle\sum_{\vec{k}} \hat{e}^1_{\vec{k}}(c^{L\dagger}_{\vec{k},-n} c^L_{\vec{k},n} + c^{R\dagger}_{\vec{k},-n} c^R_{\vec{k},n})\rangle = (\Delta^L_{cz1} + \Delta^R_{cz1})(\frac{\hat{x}+i\hat{y}}{\sqrt{2}})$

2. Polar-z EI: $\vec{\Delta}^L_{pz1} + \vec{\Delta}^R_{pz1} = \frac{g}{2\Omega}\langle\sum_{\vec{k}} \hat{e}^1_{\vec{k}}(c^{L\dagger}_{\vec{k},-n} c^L_{\vec{k},n} + c^{R\dagger}_{\vec{k},-n} c^R_{\vec{k},n})\rangle = (\Delta^L_{pz1} + \Delta^R_{pz1})\hat{z}$

3. Polar-x EI: $\vec{\Delta}^L_{px1} + \vec{\Delta}^R_{px1} = \frac{g}{2\Omega}\langle\sum_{\vec{k}} \hat{e}^1_{\vec{k}}(c^{L\dagger}_{\vec{k},-n} c^L_{\vec{k},n} + c^{R\dagger}_{\vec{k},-n} c^R_{\vec{k},n})\rangle = (\Delta^L_{px1} + \Delta^R_{px1})\hat{x}$

4. Chiral-x EI: $\vec{\Delta}^L_{cx1} + \vec{\Delta}^R_{cx1} = \frac{g}{2\Omega}\langle\sum_{\vec{k}} \hat{e}^1_{\vec{k}}(c^{L\dagger}_{\vec{k},-n} c^L_{\vec{k},n} + c^{R\dagger}_{\vec{k},-n} c^R_{\vec{k},n})\rangle = (\Delta^L_{cx1} + \Delta^R_{cx1})(\frac{\hat{y}+i\hat{z}}{\sqrt{2}})$

The number 4 comes from the fact: while vector $\hat{k}$ spans the whole unit sphere, vector $\hat{e}^1_{\vec{k}}$ only spans in the southern hemisphere, which makes the $\hat{z}$ axis be different from the other two axes. Therefore we would have one order parameter along $\hat{z}$ direction and another order parameter to be perpendicular with $\hat{z}$ direction; at the same time, we still need another two order parameters to resolve the two axes inside the xy-plane, one of which should locate inside the xy-plane, and the other one should be perpendicular with the former one and should also link the plane with the special $\hat{z}$ axis. That's why we produced the 4 vectorial order parameters listed above.

Following the similar procedure of mean field analysis approach for the inter-nodal part interaction, we can also diagonalize the hamiltonian and minimize the free energy with respect to the four order parameters. Finally we are left with a similar minimization particle-hole instabilities condition as in Eq.(2.6), where $\Delta_\alpha = 2\Delta^{R/L}_\alpha$ is the zero temperature order parameter magnitude and α denotes the four possible particle-hole instability phases. For every interaction strength g, we can calculate the corresponding order parameter magnitude Δ from the minimization particle-hole instabilities condition. After normalizing all the quantities to be dimensionless, we can produce the figure in Fig.2.4, where the magnitude of

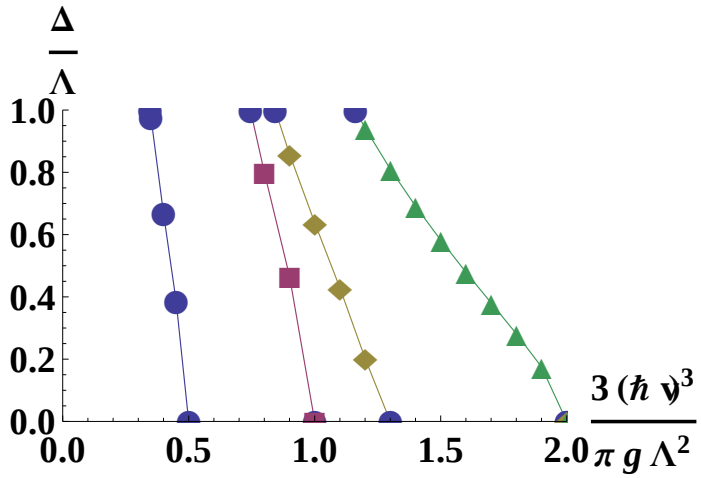

Figure 2.4: Order parameter magnitude as a function of inverse of the interaction strength for Polar-x EI Δ_{px1} (blue $\circ$), Chiral-z EI Δ_{cz1} (purple $\square$), Chiral-x EI Δ_{cx1} (brown $\Diamond$), and Polar-z EI Δ_{pz1} (green $\triangle$).

the order parameter of the four states, are plotted as a function of the interaction strength. From the plot, we see that for $g > 3(\hbar v)^3/2\pi\Lambda^2$, the polar-z EI has the largest gap for the same interaction strength among these four states. At zero temperature we get $\Delta_{pz1} > \Delta_{cx1} > \Delta_{cz1} > \Delta_{px1}$. As for the condensation energy for the four particle-hole phases related to $\hat{e}^1_{\vec{k}}$ component, we have also made the plot in Fig.2.5, where we are told this relation $E_c^{pz1} < E_c^{cx1} < E_c^{cz1} < E_c^{px1}$ for the same interaction strength g larger than $6(\hbar v)^3/\pi\Lambda^2$.

By comparing Fig.2.4 and Fig.2.5 from order parameters related to $\hat{e}^1_{\vec{k}}$ component with Fig.2.2 and Fig.2.3 from order parameters of inter-nodal part interaction, we conclude that the polar-z Excitonic Insulator phase and the chiral Charge Density Wave phase are equally energetically favorable among the six possible particle-hole states up to now for a given interaction strength. Following the same procedure of Ginzburg Landau free energy analysis, we can get the Ginzburg Landau coefficients for the polar-z Excitonic Insulator state in the following form:

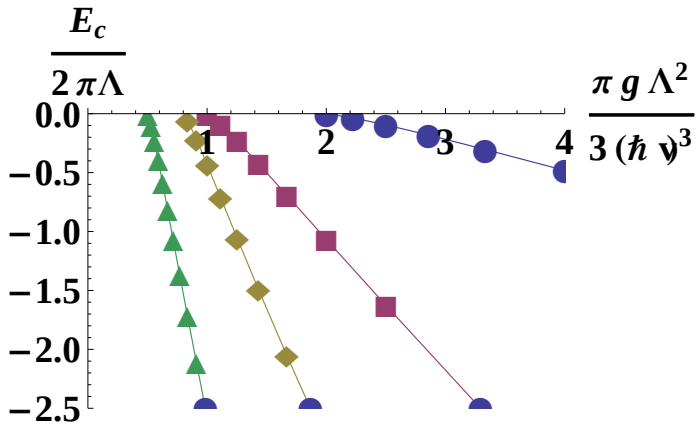

Figure 2.5: Condensation energy E_c with $\mu = 0$ as a function of the interaction strength for Polar-x EI Δ_{px1} (blue $\circ$), Chiral-z EI Δ_{cz1} (purple $\square$), Chiral-x EI Δ_{cx1} (brown $\Diamond$), and Polar-z EI Δ_{pz1} (green $\triangle$).

$$\begin{aligned} a_{pz} &\simeq \frac{2\pi}{3k_BT}\left(\frac{1}{\beta_c\hbar v}\right)^3\left(1-\frac{T}{T_c}\right) \\ b_{pz} &\simeq \frac{2\pi}{15(\hbar v)^3}\left[\frac{\beta_c\Lambda}{2}\ln 2+\frac{1}{4}\left(\ln\left(\frac{\beta_c\Lambda}{2\pi}\right)-\Psi\left(\frac{1}{2}\right)\right)\right] \end{aligned} \tag{2.18}$$

Comparing the above coefficients with Eq.(2.15), we find that $a_{pz} = \frac{1}{2}a_c$ and $b_{pz} = \frac{1}{4}b_c$, which yields a smaller order parameter in polar-z Excitonic Insulator state (only $\frac{1}{\sqrt{2}}$ that of the chiral Charge Density Wave state), but the same condensation energy as chiral Charge Density Wave phase at finite temperature. Finally we note that none of these phases gap out the Weyl node or produce any non-zero gap at Weyl nodes between the conduction bands and valence bands.

Next we focus on the order parameter of particle hole instabilities along the $\hat{e}^2_{\vec{k}}$, i.e. $\vec{\Phi}^{2*}_{\vec{k}} \cdot \vec{\Phi}^{2}_{\vec{k}'}$. There are only two possible particle-hole instabilities for order parameters related to $\hat{e}^2_{\vec{k}}$ component:

1. Polar EI: $\vec{\Delta}^L_{p2} + \vec{\Delta}^R_{p2}) = \frac{g}{2\Omega}\langle\sum_{\vec{k}} \hat{e}^2_{\vec{k}}(c^{L\dagger}_{\vec{k},-n}c^L_{\vec{k},n} - c^{R\dagger}_{\vec{k},-n}c^R_{\vec{k},n})\rangle = (\Delta^L_{p2} + \Delta^R_{p2})\hat{x}$

2. Chiral EI: $\vec{\Delta}^L_{c2} - \vec{\Delta}^R_{c2} = \frac{g}{2\Omega}\langle\sum_{\vec{k}} \hat{e}^2_{\vec{k}}(c^{L\dagger}_{\vec{k},-n}c^L_{\vec{k},n} - c^{R\dagger}_{\vec{k},-n}c^R_{\vec{k},n})\rangle = (\Delta^L_{c2} + \Delta^R_{c2})(\frac{\hat{x}+i\hat{y}}{\sqrt{2}})$

Here we have made a simplification by setting $\Delta_{p2}^R = \Delta_{p2}^L \equiv \Delta_{p2}/2 > 0$ and $\Delta_{c2}^R = \Delta_{c2}^L \equiv \Delta_{c2}/2 > 0$ under the assumption of inversion symmetry.

The reason of only two possible particle-hole instability phases is that the order parameter have different signs between the two Dirac nodes and there are two possible Excitonic Insulator states based on symmetry, as there is no z-component in $\hat{e}_{\vec{k}}^2$. So, while vector $\hat{k}$ spans the whole unit sphere, vector $\hat{e}_{\vec{k}}^2$ would only spans inside the xy-plane, which makes the $\hat{e}_{\vec{k}}^2$ component doesn't have meaningful vectorial order parameter along $\hat{z}$ axis. Therefore we would need one order parameter locate inside the xy-plane and the other one should be perpendicular with the former one and should also link the plane with the special $\hat{z}$ axis. That's why we would only have 2 vectorial order parameters listed for $\hat{e}_{\vec{k}}^2$ component.

Following the procedure of mean field analysis for the inter-nodal part interaction, we diagonalize the hamiltonian and minimize the free energy with respect to the two order parameters. Finally we are left with a similar minimization particle-hole instabilities condition as in Eq.(2.6). Here we also make the plot for the two particle-hole instabilities phases, where in order to make comparison explicitly, we have added our former data of chiral Charge Density Wave phase. For every interaction strength g, we calculate the corresponding order parameter magnitude Δ from the minimization particle-hole instabilities condition, and normalize all the quantities to be dimensionless, and plot the results in Fig.2.6. From the plot, we can see that for $g > (\hbar v)^3/\pi\Lambda^2$, there exists chiral Excitonic Insulator phase which has the largest gap for the same interaction strength among these three states.

At zero temperature we get $\Delta_{c2} > \Delta_{CDW} > \Delta_{p2}$. As for the condensation energy for the three particle-hole phases, two of which are related to $\hat{e}_{\vec{k}}^2$ component, we have also

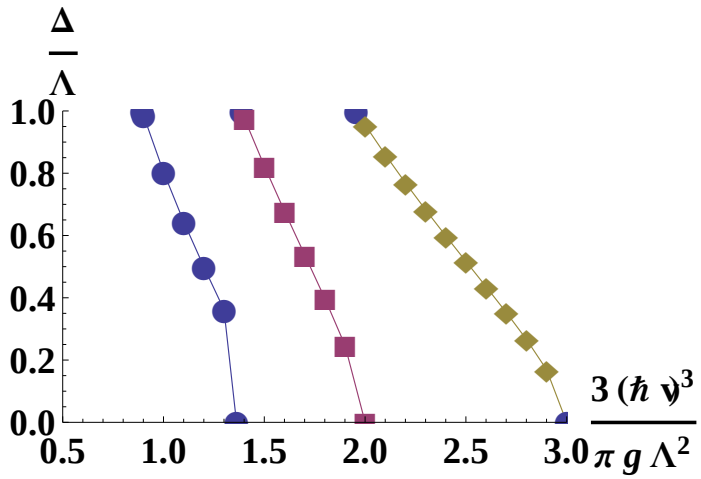

Figure 2.6: Order parameter magnitude as a function of inverse of the interaction strength for Polar EI Δ_{p2} (blue $\circ$), Chiral CDW Δ_c (purple $\square$), and Chiral EI Δ_{c2} (brown $\diamond$). Chiral CDW is shown here for comparison.

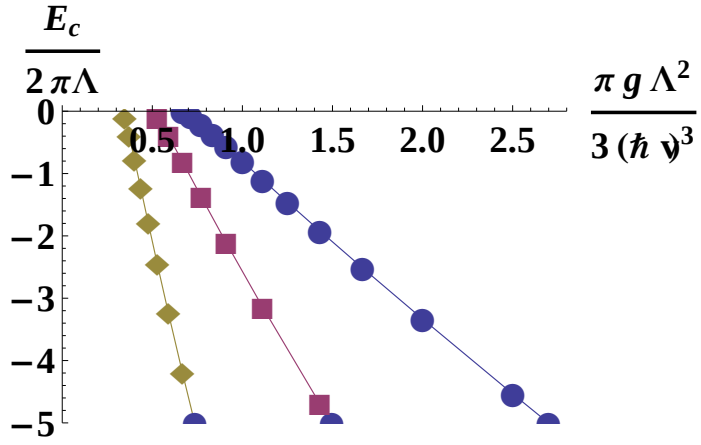

Figure 2.7: Condensation energy E_c with $\mu = 0$ as a function of the interaction strength for Polar EI Δ_{p2} (blue $\circ$), Chiral CDW Δ_c (purple $\square$), and Chiral EI Δ_{c2} (brown $\diamond$). Chiral CDW is shown here for comparison. Chiral EI is the most energetically favorable among all states.

made the plot in Fig.2.7, where we find this relation $E_c^{c2} < E_c^{CDW} < E_c^{p2}$ for the same interaction strength g larger than $2.1(\hbar v)^3/\pi\Lambda^2$.

The same conclusion can be reached analytically. Taylor expanding the gap equation (Eq.(2.6)) for $\hat{e}^2_{\vec{k}}$ case. we get

$$1 \simeq \frac{\pi g \Lambda^2}{(\hbar v)^3}\Big[1 + \left(1 + \ln\left(\frac{\Delta_{c2}^2}{8\Lambda^2}\right)\right)\frac{\Delta_{c2}^2}{4\Lambda^2} + \dots\Big] \tag{2.19}$$

We find that for $g > (\hbar v)^3/\pi\Lambda^2$ there exists a chiral Excitonic Insulator instability with a uniform gap. From Fig.2.6 we see the chiral Excitonic Insulator state has the largest gap value compared with all other states for a given interaction strength. Also Fig.2.7 shows that the chiral Excitonic Insulator state is also more energetically favorable at zero temperature compared with the chiral Charge Density Wave state or polar Excitonic Insulator phase.

We conclude that the Chiral Excitonic Insulator phase is the only state that opens a non-zero gap at the Weyl nodes. In the next section we explore its magnetic properties.

2.6 Ferromagnetic Phase of the Chiral EI State

For short-range repulsive interaction at zero temperature the chiral Excitonic Insulator phase is the most stable state among all the possible particle-hole instability states. This chiral Excitonic Insulator states mix particle and hole states which have opposite spin orientations in the non-interacting limit. Thus the superposition in the new ground state less to the spins to no longer be aligned with their momenta. In order to evaluate the nature of the spin configuration in the Weyl semimetal system, we compute the expectation value of spin at momenta $\vec{k}$ for the occupied band. The result is that there exists a net polarization for the expectation value of spin at each Weyl node. For the purpose of understanding the origin of this result, we first rotate the mean field Hamiltonian back to the $\psi_{k,\sigma}$ fermionic

basis. It takes the form :

$$H_{\pm} = H_{0\pm} - \sum_{\vec{k}} \psi^{\dagger}_{\vec{k}\alpha} \vec{\Delta}' \cdot \left[\hat{e}^2_{\vec{k}} \hat{e}^2_{\vec{k}} \mp \left(\hat{e}^2_{\vec{k}} \times \vec{n} \right) \hat{e}^1_{\vec{k}} \right] \cdot \vec{\sigma}_{\alpha\beta} \psi_{\vec{k}\beta} \tag{2.20}$$

Here we have defined a new vector: $\vec{\Delta}' = \tilde{\Delta} \sin(\chi)\, \hat{l} + \tilde{\Delta} \cos(\chi)\, \hat{m}$, and the $\tilde{\Delta}$ is the projection of the vectorial order parameter on the direction of unit vector $\hat{e}^2_{\vec{k}}$: $|\vec{\Delta}_{c2} \cdot \hat{e}^2_{\vec{k}}|$. Also the χ is the corresponding phase of the vectorial order parameter.

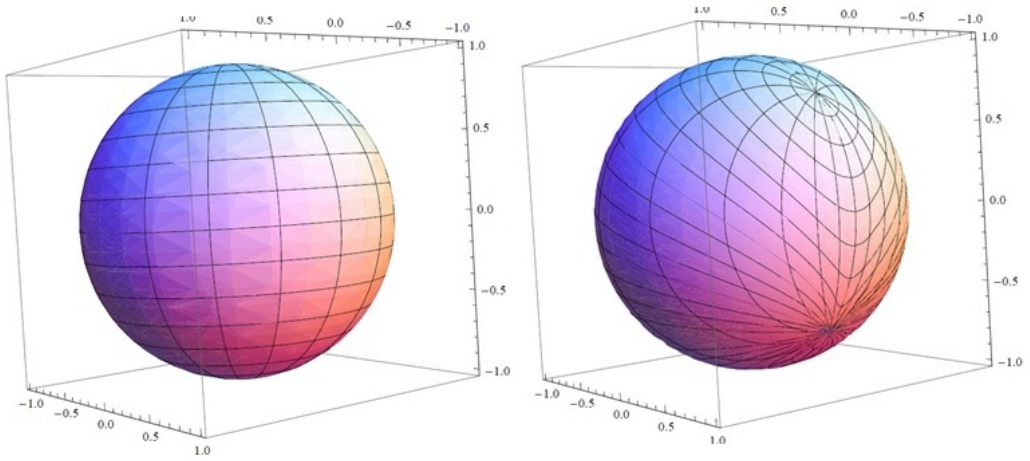

Figure 2.8: Spin direction distribution on the surface of unit sphere in reciprocal space. Left: Distribution in the non-interacting limit; Right: Distribution while a short-range repulsive interaction is applied, where we are shown that the expectation value of spin has a non-zero value. It is the origin of the magnetization in the chiral Excitonic Insulator state.

From Fig.2.1, we see that under inversion operation, $\hat{e}^1_{\vec{k}}$ does not change sign but $\hat{e}^2_{\vec{k}}$ does; on the other hand, inversion operation interchanges the two Weyl nodes (we would go from one Weyl node to the other under inversion operation). Therefore the hamiltonian preserves the inversion symmetry as the expression inside the square brackets is unchanged.

In order to get the expectation value of spin, we c averaging over polar and azimuthal angles, which leads to a term of the form $\vec{\Delta}' \cdot \vec{\sigma}/2$ at both Weyl nodes. This non-zero expectation value is the origin of the magnetization in the chiral Excitonic Insulator state

and serves as a diagnostic of this state. The spin orientation is also plotted on an equal energy surface around the node in Fig.2.8. Note that occupation of spins aligned opposite teach other is equal in the absence of the order parameter. In the presence of the order parameter there is a net canting.

The finite magnetization also provides a route to detecting this state. Hysteresis of magnetization with respect to applied field is one route. In addition, the gap can be manipulated by an external magnetic field as it couples linearly to the order parameter. As such the chiral EI phase is a rare example of a correlated ferromagnetic insulator.

Chapter 3

Excitonic Phases by Long-range Repulsive Interaction

Here we consider the effect of long-range unscreened Coulomb interaction. Our previous analysis with short-range interaction can be viewed effectively as screened Coulomb interaction the Weyl semi-metal system. The bare, unrenormalized long-range Coulomb interaction should promote the Excitonic Insulator phases or Charge Density Wave states with infinitesimal repulsive interaction, but running coupling constants modify the result yielding again a minimum cutoff value of the interaction strength to develop the Charge Density Wave phases or Excitonic Insulator states. This is similar to the two dimensional Dirac system such as graphene [44, 45].

The bare unscreened Coulomb interaction in momentum space is of the form: $V(\vec{q}) = g/|\vec{q}|^2$, where g is a positive coefficient. The dominant channels for Excitonic Insulator states and Charge Density Wave states come from the first line of Eq.(2.3) and the second term in the third line of Eq.(2.3) respectively. This is because terms involving

$2\vec{K}_0$ are much smaller than others: $|\vec{K}_0| \gg |\vec{k}|$ or $|\vec{k'}|$.

The same mean field gap equation for momentum dependent coupling is:

$$\Delta(\vec{k}) = \sum_{\vec{k'}} V(\vec{k}, \vec{k'}) \frac{\Delta(\vec{k'})}{2E_{\vec{k'}}} \tanh \frac{\beta E_{\vec{k'}}}{2} \tag{3.1}$$

with $E_{\vec{k'}} = \sqrt{(\hbar v|\vec{k'}|)^2 + |\Delta(\vec{k'})|^2}$. The Coulomb interaction in momentum space is $V(\vec{k}, \vec{k'}) = V(\vec{k} - \vec{k'}) = g/|\vec{k} - \vec{k'}|^2$. We focus on the zero temperature phased diagram, which makes the tanh factor in Eq.(3.1) to be 1. In the following two small sections, we will discuss the new phases in that are condensed.

3.1 Inter-nodal Instability: Charge Density Wave

Among the three lines in Eq.(2.3), the third line represents the inter-nodal mechanism. There are two channels with coupling constant 1 and $\hat{k} \cdot \hat{k'}$. The angle independent factor "1" is dominant in determining the magnitude of order parameters, comparing with the factor "$\hat{k} \cdot \hat{k'}$". Hence in the following, as for the inter-nodal part of interaction, we will only focus on how the factor "1" generates a uniform gap for the Charge Density Wave phase.

For this channel, Eq.(3.1) becomes:

$$\Delta(\vec{k}) = \frac{g}{2} \sum_{\vec{k'}} \frac{1}{|\vec{k} - \vec{k'}|^2} \frac{\Delta(\vec{k'})}{\sqrt{(\hbar v k')^2 + |\Delta(\vec{k'})|^2}} \tag{3.2}$$

In order to get the magnitude of the order parameter, here we expand $\Delta(\vec{k})$ in the spherical harmonics[46] as:

$$\Delta(\vec{k}) = \sum_{l=0}^{\infty} \sum_{m=-l}^{l} \Delta_l^m(|\vec{k}|) Y_l^m(\theta, \phi) \tag{3.3}$$

Also, we can do the same expansion for the $|\vec{k}-\vec{k'}|^{-1}$.We have:

$$\frac{1}{|\vec{k}-\vec{k'}|}=\sum_{l=0}^{\infty}\sum_{m=-l}^{l}\frac{4\pi}{2l+1}\frac{k_<^l}{k_>^{l+1}}Y_l^{m^*}(\theta',\phi')Y_l^m(\theta,\phi) \tag{3.4}$$

Here, $k_<$ =min($|\vec{k}|,|\vec{k'}|$) and $k_>$ =max($|\vec{k}|,|\vec{k'}|$). As the above expansion equation needs to be squared before being taken into Eq.(3.2), so the number of summation indices is doubled. Under these expansions, Eq.(3.2) becomes:

$$\begin{aligned}&\sum_{l_3m_3}\Delta_{l_3}^{m_3}(k)Y_{l_3}^{m_3{}^*}(\theta,\phi)=\\&\frac{g}{16\pi^3}\int k'^2\,dk'\int_0^{\pi}\sin\theta'\,d\theta'\int_0^{2\pi}d\phi'\sum_{l_1m_1}\sum_{l_2m_2}\left[\frac{4\pi}{2l_1+1}\frac{4\pi}{2l_2+1}\frac{k_<^{l_1}}{k_>^{l_1+1}}\frac{k_<^{l_2}}{k_>^{l_2+1}}\times\right.\\&\left.Y_{l_1}^{m_1{}^*}(\theta',\phi')Y_{l_1}^{m_1}(\theta,\phi)Y_{l_2}^{m_2{}^*}(\theta',\phi')Y_{l_2}^{m_2}(\theta,\phi)\frac{\sum_{l_4m_4}\Delta_{l_4}^{m_4}(k')Y_{l_4}^{m_4{}^*}(\theta',\phi')}{\sqrt{(\hbar vk')^2+\frac{1}{4\pi}\Delta_0^0(k')^2}}\right]\end{aligned} \tag{3.5}$$

Here, we have replaced $\sum_{\vec{k'}}$ by $\frac{1}{(2\pi)^3}\int d^3\vec{k'}$, and $\Delta(\vec{k'})$ in the denominator of Eq.(3.2) by its leading expansion term: $\Delta_0^0(k')Y_0^0(\theta',\phi')=\frac{1}{\sqrt{4\pi}}\Delta_0^0(k')$.

$$\begin{aligned}&\int d\Omega' Y_{l_1}^{m_1{}^*}(\theta',\phi')Y_{l_2}^{m_2{}^*}(\theta',\phi')Y_{l_4}^{m_4{}^*}(\theta',\phi')=\\&\sqrt{\frac{(2l_1+1)(2l_2+1)(2l_4+1)}{4\pi}}\begin{pmatrix}l_1 & l_2 & l_4\\ 0 & 0 & 0\end{pmatrix}\begin{pmatrix}l_1 & l_2 & l_4\\ m_1 & m_2 & m_4\end{pmatrix}\end{aligned} \tag{3.6}$$

Here, $\int d\Omega'=\int_0^{2\pi}d\phi'\int_0^{\pi}\sin\theta'\,d\theta'$ and $\begin{pmatrix}j_1 & j_2 & j_3\\ m_1 & m_2 & m_3\end{pmatrix}$ is a Wigner 3j-symbol[47], which is related to the Clebsch-Gordan coefficients[24]. All the parameters are integers or half-integers. Additionally, the following selection rules should also be satisfied by these parameters:

1. $m_i\in\{-|j_i|,\ldots,|j_i|\}$, $i=1,2,3$.

2. $m_1 + m_2 + m_3 = 0$

3. $|j_1 - j_2| \leqslant j_3 \leqslant j_1 + j_2$

4. $j_1 + j_2 + j_3$ should be an integer.

If any of the four selection rules is not satisfied, the Wigner 3j-symbol matrix goes to zero. Putting Eq.(3.6) into Eq.(3.5) gives:

$$\sum_{l_3 m_3} \Delta_{l_3}^{m_3}(k) Y_{l_3}^{m_3{}^*}(\theta,\phi) = \frac{g}{\pi} \int k'^2\, dk' \sum_{l_1 m_1} \sum_{l_2 m_2} \sum_{l_4 m_4} \sqrt{\frac{2l_4+1}{4\pi(2l_1+1)(2l_2+1)}} \times \begin{pmatrix} l_1 & l_2 & l_4 \\ 0 & 0 & 0 \end{pmatrix} \begin{pmatrix} l_1 & l_2 & l_4 \\ m_1 & m_2 & m_4 \end{pmatrix} \frac{k_<^{l_1+l_2}}{k_>^{l_1+l_2+2}} \frac{Y_{l_1}^{m_1}(\theta,\phi) Y_{l_2}^{m_2}(\theta,\phi) \Delta_{l_4}^{m_4}(k')}{\sqrt{(\hbar v k')^2 + \frac{1}{4\pi}\Delta_0^0(k')^2}} \tag{3.7}$$

Multiplying $Y_{l_5}^{m_5}(\theta,\phi)$ and performing the integral $\int d\Omega$ in Eq.(3.7) gives:

$$\Delta_{l_5}^{m_5}(k) = \sum_{l_1 m_1} \sum_{l_2 m_2} \sum_{l_4 m_4} \sqrt{(2l_4+1)(2l_5+1)} \begin{pmatrix} l_1 & l_2 & l_4 \\ 0 & 0 & 0 \end{pmatrix} \begin{pmatrix} l_1 & l_2 & l_4 \\ m_1 & m_2 & m_4 \end{pmatrix} \times \begin{pmatrix} l_1 & l_2 & l_5 \\ 0 & 0 & 0 \end{pmatrix} \begin{pmatrix} l_1 & l_2 & l_5 \\ m_1 & m_2 & m_5 \end{pmatrix} \frac{g}{4\pi^2} \int_0^{\frac{\Lambda}{\hbar v}} k'^2\, dk' \frac{k_<^{l_1+l_2}}{k_>^{l_1+l_2+2}} \frac{\Delta_{l_4}^{m_4}(k')}{\sqrt{(\hbar v k')^2 + \frac{1}{4\pi}\Delta_0^0(k')^2}} \tag{3.8}$$

In the LHS of Eq.(3.8), we have used the orthogonality condition of spherical harmonics:

$$\int d\Omega' Y_{l'}^{m'{}^*}(\theta,\phi) Y_l^m(\theta,\phi) = \delta_{ll'}\delta_{mm'} \tag{3.9}$$

On the RHS of Eq.(3.8), we have used Eq.(3.6). Let's focus on the dominant leading term of $\Delta(\vec{k})$ in its expansion: $\frac{1}{\sqrt{4\pi}}\Delta_0^0(k)$, which requires setting $l_5 = 0$ and $m_5 = 0$ in Eq.(3.8). According to the selection rules of Wigner 3j-symbol, the restriction on l_5 and m_5 leads to: $l_2 = l_1$, $m_2 = -m_1$, $m_4 = 0$. Considering $\begin{pmatrix} l_1 & l_1 & 0 \\ m_1 & -m_1 & 0 \end{pmatrix} = \frac{(-1)^{l_1 - m_1}}{\sqrt{2l_1+1}}$, we have the expression of $\Delta_0^0(k)$:

$$\Delta_0^0(k) = \sum_{l_1 m_1, l_4} \sqrt{2l_4+1} \begin{pmatrix} l_1 & l_1 & l_4 \\ & & \\ 0 & 0 & 0 \end{pmatrix} \begin{pmatrix} l_1 & l_1 & l_4 \\ & & \\ m_1 & -m_1 & 0 \end{pmatrix} \times \frac{(-1)^{2l_1-m_1}}{2l_1+1} \frac{g}{4\pi^2} \int \frac{k_<^{2l_1}}{k_>^{2l_1+2}} \frac{\Delta_{l_4}^0(k') k'^2 \, dk'}{\sqrt{(\hbar v k')^2 + \frac{1}{4\pi}\Delta_0^0(k')^2}} \tag{3.10}$$

For $\begin{pmatrix} l_1 & l_1 & l_4 \\ & & \\ 0 & 0 & 0 \end{pmatrix} \cdot \begin{pmatrix} l_1 & l_1 & l_4 \\ & & \\ m_1 & -m_1 & 0 \end{pmatrix}$ factor, its value with $l_4 = 0$ is much larger than that its value with $l_4 \neq 0$. Therefore only keep the $l_4 = 0$ terms in $\sum_{l_4}$ while calculating $\Delta_0^0(k)$ in Eq.(3.10), which results in:

$$\begin{aligned} \Delta_0^0(k) &= \frac{g}{4\pi^2} \int_0^{\frac{\Lambda}{\hbar v}} \left(\sum_{l_1} \frac{k'^2}{2l_1+1} \frac{k_<^{2l_1}}{k_>^{2l_1+2}} \right) \frac{\Delta_0^0(k') \, dk'}{\sqrt{(\hbar v k')^2 + \frac{1}{4\pi}\Delta_0^0(k')^2}} \\ &= \frac{g}{4\pi^2} \left[\int_0^k \sum_{l_1} \frac{(k'/k)^{2l_1+2}}{2l_1+1} \frac{\Delta_0^0(k') \, dk'}{\sqrt{(\hbar v k')^2 + \frac{1}{4\pi}\Delta_0^0(k')^2}} \right. \\ &\quad \left. + \int_k^{\frac{\Lambda}{\hbar v}} \sum_{l_1} \frac{(k/k')^{2l_1}}{2l_1+1} \frac{\Delta_0^0(k') \, dk'}{\sqrt{(\hbar v k')^2 + \frac{1}{4\pi}\Delta_0^0(k')^2}} \right] \end{aligned} \tag{3.11}$$

Here we have used $\sum_{m_1} = 2l_1 + 1$, given that the summation function is independent of m_1. Expand the summation $\sum_{l_1}$ to $l_1 = 1$ in Eq.(3.11), we have:

$$\begin{aligned} \Delta_0^0(k) = \frac{g}{4\pi^2} \Bigg[& \int_0^k \left[(\frac{k'}{k})^2 + \frac{1}{3} (\frac{k'}{k})^4 \right] \frac{\Delta_0^0(k') \, dk'}{\sqrt{(\hbar v k')^2 + \frac{1}{4\pi}\Delta_0^0(k')^2}} \\ & + \int_k^{\frac{\Lambda}{\hbar v}} \left[1 + \frac{1}{3} (\frac{k}{k'})^2 \right] \frac{\Delta_0^0(k') \, dk'}{\sqrt{(\hbar v k')^2 + \frac{1}{4\pi}\Delta_0^0(k')^2}} \Bigg] \end{aligned} \tag{3.12}$$

Here we find $l_1 = 1$ term is much smaller than $l_1 = 0$ term, so keeping the dominant $l_1 = 0$ term is enough. This yields:

$$\Delta_0^0(k) = \frac{g}{4\pi^2} \int_0^k \frac{k'^2}{k^2} \frac{\Delta_0^0(k') dk'}{\sqrt{(\hbar v k')^2 + \frac{1}{4\pi}\Delta_0^0(k')^2}} + \frac{g}{4\pi^2} \int_k^{\frac{\Lambda}{\hbar v}} \frac{\Delta_0^0(k') dk'}{\sqrt{(\hbar v k')^2 + \frac{1}{4\pi}\Delta_0^0(k')^2}} \tag{3.13}$$

After rescaling the parameters $u = \hbar v k$ and $u' = \hbar v k'$, we can simplify the above equation to:

$$\Delta_0^0(u) = \frac{g}{4\pi^2\hbar v}\int_0^u \left(\frac{u'}{u}\right)^2 \frac{\Delta_0^0(u')du'}{\sqrt{u'^2 + \frac{1}{4\pi}\Delta_0^0(u')^2}} + \frac{g}{4\pi^2\hbar v}\int_u^\Lambda \frac{\Delta_0^0(u')du'}{\sqrt{u'^2 + \frac{1}{4\pi}\Delta_0^0(u')^2}} \tag{3.14}$$

Next, we calculate the leading term $\Delta_0^0(u)$ from Eq.(3.14). Taking derivatives with respect to u on the two sides of Eq.(3.14) gives:

$$\frac{d\Delta(u)}{du} = \frac{-2}{u}\left(\Delta(u) - \frac{g}{4\pi^2\hbar v}\int_u^\Lambda \frac{\Delta(u')du'}{\sqrt{u'^2 + \frac{1}{4\pi}\Delta(u')^2}}\right) \tag{3.15}$$

Here we have neglected all the subscript and superscript in $\Delta_0^0(u)$. Multiplying u on two sides of above equation and taking derivative with respect to u again gives:

$$u\frac{d^2\Delta(u)}{du^2} + 3\frac{d\Delta(u)}{du} + \frac{g}{2\pi^2\hbar v}\frac{\Delta(u)}{\sqrt{u^2 + \frac{1}{4\pi}\Delta(u)^2}} = 0 \tag{3.16}$$

In order to extract useful information from Eq.(3.14), we make the following assumption for simplifying order parameter's calculation[44]: the dominant contribution to $\Delta_0^0(k)$ comes from the region of $u' \in [u^*, \Lambda]$, where u^* is determined by the condition $u^* = \Delta(u^*)/\sqrt{4\pi}$, and we can neglect the contribution from the region of $u' \in [0, u^*]$. The validity of this approach is demonstrated in the function dependence shown in Fig.(3.1). This condition allow us to simplify Eq.(3.14) and Eq.(3.16) to:

$$\Delta_0^0(u) = \frac{g}{4\pi^2\hbar v}\int_{u^*}^u du'\left(\frac{u'}{u}\right)^2 \frac{\Delta_0^0(u')}{u'} + \frac{g}{4\pi^2\hbar v}\int_u^\Lambda du' \frac{\Delta_0^0(u')}{u'} \tag{3.17}$$

and

$$u^2\frac{d^2\Delta(u)}{du^2} + 3u\frac{d\Delta(u)}{du} + \frac{g}{2\pi^2\hbar v}\Delta(u) = 0 \tag{3.18}$$

General solution for Eq.(3.18) can be written in the following form:

$$\Delta(u) = Au^{-1-\sqrt{1-\frac{g}{2\pi^2\hbar v}}} + Bu^{-1+\sqrt{1-\frac{g}{2\pi^2\hbar v}}} \tag{3.19}$$

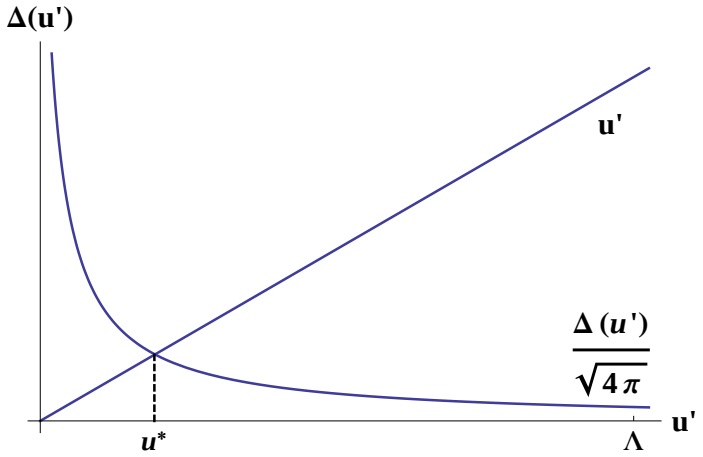

Figure 3.1: the determination of u^*, which split the integration region into two parts: the small u' region is neglected, while the other region is taken to be the dominant one.

From Eq.(3.17), we have the boundary conditions for the differential equation:

$$\begin{aligned} u^3 \frac{d\Delta(u)}{du}\bigg|_{u\to u^*} &= 0 \\ \left(u\frac{d\Delta(u)}{du} + 2\Delta(u)\right)\bigg|_{u\to\Lambda} &= 0 \end{aligned} \tag{3.20}$$

Taking the general solution into the boundary conditions, we are left with:

$$\frac{u^*}{\Lambda} = \left(\frac{1+\sqrt{1-\frac{g}{2\pi^2\hbar v}}}{1-\sqrt{1-\frac{g}{2\pi^2\hbar v}}}\right)^{\frac{1}{\sqrt{1-\frac{g}{2\pi^2\hbar v}}}} \tag{3.21}$$

If g is a very small, then we find $u^* \gg \Lambda$, which violates our assumption that u^* should be much smaller comparing with the upper cutoff value of the integral on $\vec{k}$: Λ. Thus no physical solution exists for small. One requires should be large enough to make $1-\frac{g}{2\pi^2\hbar v}$ be negative. Defining $\sqrt{1-\frac{g}{2\pi^2\hbar v}} = i\alpha$ with $\alpha = \sqrt{\frac{g}{2\pi^2\hbar v}-1} > 0$, and rewriting Eq.(3.21), we have:

$$\frac{u^*}{\Lambda} = \left(\frac{1+i\alpha}{1-i\alpha}\right)^{\frac{1}{i\alpha}} = e^{\frac{1}{i\alpha}\ln\frac{1+i\alpha}{1-i\alpha}} \tag{3.22}$$

Considering the modulus of $\frac{1+i\alpha}{1-i\alpha}$ is 1, thus it is appropriate to assume that it is

equal to $e^{i\varphi}$, then we have:

$$\frac{u^*}{\Lambda} = e^{\frac{\varphi}{\alpha}} \tag{3.23}$$

Here we can find that: $\frac{u^*}{\Lambda} < 1$ requires $\frac{\varphi}{\alpha} < 0$, which leads to $\varphi < 0$, because $\alpha = \sqrt{\frac{g}{2\pi^2\hbar v} - 1}$ is always positive.

On the other hand, we know: $\cos\varphi = \frac{1-\alpha^2}{1+\alpha^2}$ and $\sin\varphi = \frac{2\alpha}{1+\alpha^2}$ where $\alpha > 0$, which gives $\cos\varphi \in (-1, 1)$ and $\sin\varphi \in (0, 1)$. Therefore, $\varphi \in \big(-2n\pi, -(2n-1)\pi \big)$, with $n = 1, 2, 3\ldots$ Thus the restriction on g takes the form $\frac{g}{2\pi^2\hbar v} - 1 > 0$ or equivalently $g > 2\pi^2\hbar v$.

Further simplifications is aided by the α dependence of ϕ: $\varphi = -2n\pi + \cos^{-1}\left(\frac{1-\alpha^2}{1+\alpha^2}\right)$. This makes the ratio of u^* and Λ to be:

$$\frac{u^*}{\Lambda} = e^{\frac{-2n\pi + \arccos\left(\frac{4\pi^2\hbar v}{g} - 1\right)}{\sqrt{\frac{g}{2\pi^2\hbar v} - 1}}} \tag{3.24}$$

where $n = 1, 2, 3\ldots$

Thus, even for long range interaction the inter nodal instabilities require a minimum interaction strength for chemical potential at the node. Unlike the short range case where repulsion does not stabilize a gapped CDW, it is indeed a possible ground state for unscreened Coulomb interaction.

3.2 Intra-nodal Interaction: Excitonic Insulator

Here we focus our analysis on the intra-nodal part interaction. Like we did in the inter-nodal case, in the first line of Eq.(2.3), we first identify the most dominant channel.

In the general expression of Eq.(2.3), except the third line, both of the other two

lines in Eq.(2.3) correspond to intra-nodal part interactions, which reads:

$$
\begin{aligned}
V_{intra} = & -\sum_{\vec{k},\vec{k}',n=\pm} \times \\
& \left[V(\vec{k}-\vec{k}') \frac{\hat{e}_{\vec{k}} \cdot \hat{e}^*_{\vec{k}'} + \hat{e}^*_{\vec{k}} \cdot \hat{e}_{\vec{k}'}}{4} \sum_{\tau=R,L} c^{\tau\dagger}_{\vec{k},n} c^{\tau}_{\vec{k},-n} c^{\tau\dagger}_{\vec{k}',-n} c^{\tau}_{\vec{k}',n} \right. \\
& \left. + V(\vec{k}-\vec{k}'-2\vec{K}_0) \frac{\hat{e}_{\vec{k}} \cdot \hat{e}_{\vec{k}'} + \hat{e}^*_{\vec{k}} \cdot \hat{e}^*_{\vec{k}'}}{2} c^{L\dagger}_{\vec{k},n} c^{L}_{\vec{k},-n} c^{R\dagger}_{\vec{k}',-n} c^{R}_{\vec{k}',n} \right]
\end{aligned}
\tag{3.25}
$$

with $\hat{e}_{\vec{k}} = \hat{e}^1_{\vec{k}} + i\hat{e}^2_{\vec{k}}$.

The first term dominates, because $|\vec{k}| \ll |\vec{K}_0|$, $|\vec{k}'| \ll |\vec{K}_0|$ and $V(\vec{q})$ is inverse proportional to $\vec{q}^2$. Therefore we drop the second term and focus on the instability due to small $\vec{k}-\vec{k}'$. The coefficient in the first line is expanded in the spherical coordinate system as:

$$
\hat{e}_{\vec{k}} \cdot \hat{e}^*_{\vec{k}'} + \hat{e}^*_{\vec{k}} \cdot \hat{e}_{\vec{k}'} = 2\sin\theta\sin\theta' + 2(1+\cos\theta\cos\theta')\cos(\phi-\phi') \tag{3.26}
$$

Since we will average over the angles, it is clear that the terms with the least variation will promote the strongest instability. Of the three, the term proportional to $2\cos(\phi-\phi')$ is expected to dominate, which means the other two terms depending on θ and θ' can be safely ignored. Thus Eq.(3.25) will become:

$$
\begin{aligned}
V_{intra} = & -\sum_{\vec{k},\vec{k}'} V(\vec{k}-\vec{k}') \frac{\cos(\phi-\phi')}{2} \times \\
& \sum_{\tau=R,L} \left(c^{\tau\dagger}_{\vec{k}+} c^{\tau}_{\vec{k}-} c^{\tau\dagger}_{\vec{k}'-} c^{\tau}_{\vec{k}'+} + c^{\tau\dagger}_{\vec{k}-} c^{\tau}_{\vec{k}+} c^{\tau\dagger}_{\vec{k}'+} c^{\tau}_{\vec{k}'-} \right)
\end{aligned}
\tag{3.27}
$$

Here we have expanded the summation on n.

Within mean field[28][42], taking $\Delta(\vec{k}) = \left\langle c^{\tau\dagger}_{\vec{k}+} c^{\tau}_{\vec{k}-} \right\rangle$ would lead the bracket in the above equation to be: $\Delta(\vec{k})\Delta(\vec{k}')^* + \Delta(\vec{k})^*\Delta(\vec{k}')$, where two terms are equal if we switch $\vec{k}$, $\vec{k}'$ in one term. So the two terms can be replaced by one of them being multiplied by a

factor of 2, which shows:

$$V_{intra} = -\sum_{\vec{k},\vec{k'}} V(\vec{k}-\vec{k'})\cos(\phi-\phi') \sum_{\tau=R,L} c^{\tau\dagger}_{\vec{k}+} c^{\tau}_{\vec{k}-} c^{\tau\dagger}_{\vec{k'}-} c^{\tau}_{\vec{k'}+} \tag{3.28}$$

Now, under this expression of interaction, the self-consistent gap equation of Eq.(3.1) changes to:

$$\Delta(\vec{k}) = g\sum_{\vec{k'}} \frac{\cos(\phi-\phi')}{|\vec{k}-\vec{k'}|^2} \frac{\Delta(\vec{k'})}{2\sqrt{(\hbar v|\vec{k'}|)^2+|\Delta(\vec{k'})|^2}} \tag{3.29}$$

Expanding $\cos(\phi-\phi')$, we get become:

$$\Delta(\vec{k}) = \frac{g}{4}\sum_{\vec{k'}} \frac{e^{i\phi}e^{-i\phi'}+e^{-i\phi}e^{i\phi'}}{|\vec{k}-\vec{k'}|^2} \frac{\Delta(\vec{k'})}{\sqrt{(\hbar v|\vec{k'}|)^2+|\Delta(\vec{k'})|^2}} \tag{3.30}$$

Here the two exponential factors have equal contribution to the magnitude of order parameter Δ, so we will only keep the first factor. Assuming $\Delta(\vec{k}) = \Delta(k)e^{i\phi}$, the above self-consistent gap equation becomes:

$$\Delta(k) = \frac{g}{4}\sum_{\vec{k'}} \frac{1}{|\vec{k}-\vec{k'}|^2} \frac{\Delta(k')}{\sqrt{(\hbar v|\vec{k'}|)^2+\Delta(k')^2}} \tag{3.31}$$

It is worthwhile to note that Eq.(3.31) is very similar to Eq.(3.2), which is the self-consistent gap equation for the inter-nodal interaction case. The only difference between these two self-consistent gap equations is the right hand side of Eq.(3.31) is only half of that of Eq.(3.2). Therefore we adapt the same technique as the previous section to analyze the intra nodal case.

Taking Eq.(3.4) into Eq.(3.31), and rearrange the factors, we have:

$$\begin{aligned}\Delta(k) =& \frac{g}{32\pi^3}\sum_{l_1m_1}\sum_{l_2m_2} \frac{4\pi}{2l_1+1}\frac{4\pi}{2l_2+1} Y_{l_1}^{m_1}(\theta,\phi)Y_{l_2}^{m_2}(\theta,\phi)\times \\ & \int d\Omega' {Y_{l_1}^{m_1}}^*(\theta',\phi'){Y_{l_2}^{m_2}}^*(\theta',\phi') \int \frac{k_<^{l_1+l_2}}{k_>^{l_1+l_2+2}} \frac{\Delta(k')k'^2dk'}{\sqrt{(\hbar vk')^2+\Delta(k')^2}}\end{aligned} \tag{3.32}$$

The integration, $\int d\Omega'$, is evaluated by taking $l_4 = m_4 = 0$ in Eq.(3.6). The result is:

$$\int d\Omega' {Y_{l_1}^{m_1}}^*(\theta', \phi') {Y_{l_2}^{m_2}}^*(\theta', \phi') = (-1)^{2l_1 - m_1} \delta_{l_2, l_1} \delta_{m_2, -m_1} \tag{3.33}$$

Replacing in Eq.(3.32) the summation $\sum_{l_2 m_2}$ vanishes. Using symmetry properties of spherical Harmonics, $Y_{l_2}^{m_2}(\theta, \phi) = Y_{l_1}^{-m_1}(\theta, \phi) = (-1)^{m_1} {Y_{l_1}^{m_1}}^*(\theta, \phi)$, and the identity:

$$\sum_{m=-l}^{l} |Y_l^m(\theta, \phi)|^2 = \frac{2l+1}{4\pi} \tag{3.34}$$

Eq.(3.32) simplifies to:

$$\Delta(k) = \frac{g}{32\pi^3} \sum_l \frac{4\pi}{2l+1} \int \frac{k_<^{2l}}{k_>^{2l+2}} \frac{\Delta(k') k'^2 dk'}{\sqrt{(\hbar v k')^2 + \Delta(k')^2}} \tag{3.35}$$

Here we have replaced (l_1, m_1) with (l, m) as required by the delta functions. Using the relation between k and k', we can split the integral range into two regions. With these considerations the gap equation is

$$\begin{aligned} \Delta(k) &= \frac{g}{8\pi^2} \int_0^{\frac{\Lambda}{\hbar v}} \left(\sum_{l=0}^{\infty} \frac{k'^2}{2l+1} \frac{k_<^{2l}}{k_>^{2l+2}} \right) \frac{\Delta(k') dk'}{\sqrt{(\hbar v k')^2 + \Delta(k')^2}} \\ &= \frac{g}{8\pi^2} \left[\int_0^{k} \left(\sum_{l=0}^{\infty} \frac{1}{2l+1} \Big(\frac{k'}{k}\Big)^{2l+2} \right) \frac{\Delta(k') dk'}{\sqrt{(\hbar v k')^2 + \Delta(k')^2}} \right. \\ &\qquad \left. + \int_k^{\frac{\Lambda}{\hbar v}} \left(\sum_{l=0}^{\infty} \frac{1}{2l+1} \Big(\frac{k}{k'}\Big)^{2l} \right) \frac{\Delta(k') dk'}{\sqrt{(\hbar v k')^2 + \Delta(k')^2}} \right] \end{aligned} \tag{3.36}$$

The expansion of $\sum_{l=0}^{\infty}$ is dominated by the $l = 0$ term. Thus we neglect all the $l \neq 0$ terms, while keeping $l = 0$ term only, which gives:

$$\Delta(k) = \frac{g}{8\pi^2} \left[\int_0^{k} \Big(\frac{k'}{k}\Big)^2 \frac{\Delta(k') dk'}{\sqrt{(\hbar v k')^2 + \Delta(k')^2}} + \int_k^{\frac{\Lambda}{\hbar v}} \frac{\Delta(k') dk'}{\sqrt{(\hbar v k')^2 + \Delta(k')^2}} \right] \tag{3.37}$$

Following the procedure we did in last section for inter-nodal interactions, rescaling the parameters: $u = \hbar v k$ and $u' = \hbar v k'$ simplifies above equation to be:

$$\Delta(u) = \frac{g}{8\pi^2 \hbar v} \left[\int_0^{u} \Big(\frac{u'}{u}\Big)^2 \frac{\Delta(u') du'}{\sqrt{u'^2 + \Delta(u')^2}} + \int_u^{\Lambda} \frac{\Delta(u') du'}{\sqrt{u'^2 + \Delta(u')^2}} \right] \tag{3.38}$$

Taking two times of derivative with respect to the new variable u, we get the differential equation corresponding to the above self-consistent gap equation:

$$u\frac{d^2\Delta(u)}{du^2} + 3\frac{d\Delta(u)}{du} + \frac{g}{4\pi^2\hbar v}\frac{\Delta(u)}{\sqrt{u^2+\Delta(u)^2}} = 0 \tag{3.39}$$

Taking the similar assumption as in Fig.(3.1), and introducing u^* which is determined by $u^* = \Delta(u^*)$, we have Eq.(3.39) to be simplified:

$$u^2\frac{d^2\Delta(u)}{du^2} + 3u\frac{d\Delta(u)}{du} + \frac{g}{4\pi^2\hbar v}\Delta(u) = 0 \tag{3.40}$$

The general solution of above differential equation is obtained in the following form:

$$\Delta(u) = Au^{-1-\sqrt{1-\frac{g}{4\pi^2\hbar v}}} + Bu^{-1+\sqrt{1-\frac{g}{4\pi^2\hbar v}}} \tag{3.41}$$

This general solution satisfies the boundary condition Eq.(3.20), which is also the boundary condition of inter-nodal interaction's dominant term '1'. Since the boundary conditions are identical much of the procedure is the same as before. We get the ratio of u^* over Λ as:

$$\frac{u^*}{\Lambda} = \left(\frac{1+\sqrt{1-\frac{g}{4\pi^2\hbar v}}}{1-\sqrt{1-\frac{g}{4\pi^2\hbar v}}}\right)^{\frac{1}{\sqrt{1-\frac{g}{4\pi^2\hbar v}}}} \tag{3.42}$$

Looking for a physically meaningful solution yields a requirement of$g > 4\pi^2\hbar v$, Thus, the minimum cutoff for the excitonic insulating state for the Coulomb case is twice as large. This can be traced back to the angular dependence of the order parameter. In the CDW phase the order parameter is uniform while in here it is with $\cos(\phi)$ or $\sin(\phi)$. An averaging yields a factor of 2. Thus one expect the CDW to be the preferred ground state.

3.3 Ginzburg-Landau Free Energy Analysis

In this section we derive the Ginzburg Landau Free energies and expand on the results obtain within mean field. The Hamiltonian of the Weyl semi-metal system is

$$H_0 = \sum_{n,\vec{k}} \left(c^{L\dagger}_{n,\vec{k}} \hbar v n |\vec{k}| c^{L}_{n,\vec{k}} + c^{R\dagger}_{-n,\vec{k}} (-\hbar v n |\vec{k}|) c^{R}_{-n,\vec{k}} \right) \tag{3.43}$$

In Eq.(2.3)'s inter-nodal part, the Coulomb interaction has two terms $V(2\vec{K}_0)$ and $V(\vec{k} - \vec{k'})\hat{k} \cdot \hat{k'}$. The former can be ignored compared with the leading term $V(\vec{k} - \vec{k'})$. We write the inter-nodal part of Coulomb interaction from Eq.(2.3) in the following form:

$$V_{eff} = -\sum_{\vec{k},\vec{k'}} \sum_{n=\pm} V(\vec{k} - \vec{k'}) c^{L\dagger}_{n,\vec{k}} c^{R}_{-n,\vec{k}} c^{R\dagger}_{-n,\vec{k'}} c^{L}_{n,\vec{k'}} \tag{3.44}$$

Here $V(\vec{k} - \vec{k'}) = g/|\vec{k} - \vec{k'}|^2$ is the Coulomb interaction. In order to the usage of mean-field analysis, we define $\Psi(\vec{k'}) = \langle c^{R\dagger}_{-n,\vec{k'}} c^{L}_{n,\vec{k'}} \rangle$, and replace the creation-annihilation operator pairs by their average value $\Psi(\vec{k'})$ or $\Psi^\dagger(\vec{k})$ plus small fluctuations. The Coulomb interaction becomes:

$$V_{eff} = -\sum_{\vec{k},\vec{k'}} \sum_{n=\pm} \frac{g}{|\vec{k} - \vec{k'}|^2} \left[\Psi^\dagger(\vec{k}) c^{R\dagger}_{-n,\vec{k'}} c^{L}_{n,\vec{k'}} + \Psi(\vec{k'}) c^{L\dagger}_{n,\vec{k}} c^{R}_{-n,\vec{k}} - \Psi^\dagger(\vec{k}) \Psi(\vec{k'}) \right] \tag{3.45}$$

Here we have neglected the higher orders in the devotion from mean field[28][42]. The order parameter is

$$\Delta(\vec{k}) = \sum_{\vec{k'}} \frac{g}{|\vec{k} - \vec{k'}|^2} \Psi(\vec{k'}) \tag{3.46}$$

Similarly, we also have the expression for $\Delta^\dagger(\vec{k'})$, both of which transform the Coulomb interaction to be:

$$V_{eff} = -\sum_{n,\vec{k'}} \Delta^\dagger(\vec{k'}) c^{R\dagger}_{-n,\vec{k'}} c^{L}_{n,\vec{k'}} - \sum_{n,\vec{k}} \Delta(\vec{k}) c^{L\dagger}_{n,\vec{k}} c^{R}_{-n,\vec{k}} + \sum_{\vec{k},\vec{k'}} \sum_{n=\pm} \frac{g}{|\vec{k} - \vec{k'}|^2} \Psi^\dagger(\vec{k}) \Psi(\vec{k'}) \tag{3.47}$$

In order to write the Hamiltonian $H = H_0 + V_{eff}$ to be more compact, we replace the summation index $\vec{k'}$ by $\vec{k}$ in the first term of above equation. After that we have our full Hamiltonian in the following:

$$\begin{aligned} H = &\sum_{n,\vec{k}} \Big[c^{L\dagger}_{n,\vec{k}}(\hbar v n|\vec{k}|)c^{L}_{n,\vec{k}} - c^{L\dagger}_{n,\vec{k}}\Delta(\vec{k})c^{R}_{-n,\vec{k}} - c^{R\dagger}_{-n,\vec{k}}\Delta^{\dagger}(\vec{k})c^{L}_{n,\vec{k}} \\ &+ c^{R\dagger}_{-n,\vec{k}}(-\hbar v n|\vec{k}|)c^{R}_{-n,\vec{k}} \Big] + \sum_{\vec{k},\vec{k'}}\sum_{n=\pm} \frac{g}{|\vec{k}-\vec{k'}|^2}\Psi^{\dagger}(\vec{k})\Psi(\vec{k'}) \end{aligned} \tag{3.48}$$

Writing in the matrix form we get a 2×2 Hamiltonian similar to Eq.(2.5):

$$H = \sum_{n,\vec{k}} \begin{pmatrix} c^{L}_{n,\vec{k}} \\ c^{R}_{-n,\vec{k}} \end{pmatrix}^{\dagger} \begin{pmatrix} \hbar v n|\vec{k}| & -\Delta(\vec{k}) \\ -\Delta^{\dagger}(\vec{k}) & -\hbar v n|\vec{k}| \end{pmatrix} \begin{pmatrix} c^{L}_{n,\vec{k}} \\ c^{R}_{-n,\vec{k}} \end{pmatrix} + \sum_{\vec{k},\vec{k'}}\sum_{n=\pm} \frac{g}{|\vec{k}-\vec{k'}|^2}\Psi^{\dagger}(\vec{k})\Psi(\vec{k'}) \tag{3.49}$$

The two differences with Eq.(2.5) are: i) The definition of order parameter Δ, and ii) The constant term coming from the mean-field analysis. However, both these differences do not mitigate form an analytic computation. Employing the Bogoliubov transformation[28]:

$$\begin{pmatrix} a_{n,\vec{k}} \\ b_{n,\vec{k}} \end{pmatrix} = \begin{pmatrix} \frac{1}{c_1} & \frac{\hbar v n|\vec{k}| - \sqrt{(\hbar v n|\vec{k}|)^2 + |\Delta(\vec{k})|^2}}{c_1\Delta^{\dagger}(\vec{k})} \\ \frac{1}{c_2} & \frac{\hbar v n|\vec{k}| + \sqrt{(\hbar v n|\vec{k}|)^2 + |\Delta(\vec{k})|^2}}{c_2\Delta^{\dagger}(\vec{k})} \end{pmatrix} \begin{pmatrix} c^{L}_{n,\vec{k}} \\ c^{R}_{-n,\vec{k}} \end{pmatrix} \tag{3.50}$$

where the coefficients are:

$$c_{1,2} = \sqrt{1 + \left(\frac{\hbar v n|\vec{k}|}{|\Delta(\vec{k})|} \mp \sqrt{\left(\frac{\hbar v n|\vec{k}|}{|\Delta(\vec{k})|}\right)^2 + 1} \right)^2}, \tag{3.51}$$

the Hamiltonian is:

$$H = \sum_{n,\vec{k}} \begin{pmatrix} a_{n,\vec{k}} \\ b_{n,\vec{k}} \end{pmatrix}^{\dagger} \begin{pmatrix} E_1 & 0 \\ 0 & E_2 \end{pmatrix} \begin{pmatrix} a_{n,\vec{k}} \\ b_{n,\vec{k}} \end{pmatrix} + \sum_{\vec{k},\vec{k'}}\sum_{n=\pm} \frac{g}{|\vec{k}-\vec{k'}|^2}\Psi^{\dagger}(\vec{k})\Psi(\vec{k'}) \tag{3.52}$$

The eigenvalues of the Hamiltonian are:

$$E_{1,2} = \pm\sqrt{\left(\hbar v n|\vec{k}|\right)^2 + |\Delta(\vec{k})|^2} \tag{3.53}$$

Next, we obtain the free energy of the state, and compare with the free energy of the normal state, where the order parameter is zero. Starting from the general free energy expression, the detailed form can be retrieved as follows:

$$\begin{aligned} F &= -\frac{1}{\beta}\ln Tr\left(e^{-\beta H}\right) \\ &= -\frac{1}{\beta}\sum_{\alpha,\vec{k}}\ln\left(1+e^{-\beta E_{\alpha,\vec{k}}}\right)+H_c \end{aligned} \tag{3.54}$$

Here $\alpha = 1, 2$ represent the two energy eigenvalues, and the last part is the constant term which comes from the mean-field analysis and contributes to the condensation energy:

$$H_c = \sum_{\vec{k},\vec{k'}}\sum_{n=\pm}\frac{g}{|\vec{k}-\vec{k'}|^2}\Psi^{\dagger}(\vec{k})\Psi(\vec{k'}) \tag{3.55}$$

It is worth noting that the above free energy expression can also be obtained from another path as follows[28]:

$$\begin{aligned} F =& E - TS \\ E =& \sum_{\alpha,\vec{k}} E_{\alpha,\vec{k}} f + H_c \\ S =& -k_B\sum_{\alpha,\vec{k}}\left[(1-f)\ln(1-f)+f\ln f\right] \end{aligned} \tag{3.56}$$

Here the function f is the Fermi statistics function:

$$f\left(E_{\alpha,\vec{k}}\right) = \frac{1}{1+\exp\left(\beta E_{\alpha,\vec{k}}\right)} \tag{3.57}$$

Take the second and third line into the first, the free energy expression is obtained. Now, we calculate the condensation energy :

$$F_{CN} = F_{CDW} - F_N = -\frac{1}{\beta}\sum_{n,\alpha,\vec{k}}\ln\frac{1+e^{-\beta E_{\alpha,\vec{k}}}}{1+e^{-\beta\hbar v|\vec{k}_\alpha|}}+H_c \tag{3.58}$$

In order to get F_{CN}'s power series in $\Delta(\vec{k})$, we first take a derivative with respect to $\Delta^{\dagger}(\vec{k})$ and then perform a Taylor expansion[48] with respect to $\Delta(\vec{k})$. Finally we performs an integration on $\Delta(\vec{k})$ which gives us the F_{CN}'s power series in $\Delta(\vec{k})$. This procedure is employed below.

$$\frac{\partial F_{_{CN}}}{\partial \Delta^{\dagger}(\vec{k})} = \sum_{n,\vec{k}} \frac{\Delta(\vec{k})}{2} \Big(\sum_{\alpha} \frac{f\big(E_{\alpha,\vec{k}}\big)}{E_{\alpha,\vec{k}}} \Big) + \frac{\partial H_c}{\partial \Delta^{\dagger}(\vec{k})} \tag{3.59}$$

The terms in the bracket can be evaluated using the identity:

$$\sum_{\alpha} \frac{f\big(E_{\alpha,\vec{k}}\big)}{E_{\alpha,\vec{k}}} = \frac{-1}{E_{\vec{k}}} \tanh \frac{\beta E_{\vec{k}}}{2} \tag{3.60}$$

where $E_{\vec{k}}$ is the shortened form of $E_{\alpha=1,\vec{k}}$. The partial derivative of the condensation energy is:

$$\frac{\partial H_c}{\partial \Delta^{\dagger}(\vec{k})} = \sum_{n,\vec{k}} \Psi(\vec{k}) \tag{3.61}$$

Using these results the derivative becomes:

$$\frac{\partial F_{_{CN}}}{\partial \Delta^{\dagger}(\vec{k})} = \sum_{n,\vec{k}} \frac{-\Delta(\vec{k})}{2E_{\vec{k}}} \tanh \frac{\beta E_{\vec{k}}}{2} + \sum_{n,\vec{k}} \Psi(\vec{k}) \tag{3.62}$$

The last term needs further simplification. We return to the self-consistent particle-hole instability equation:

$$\Delta(\vec{k}) = \sum_{\vec{k'}} V(\vec{k} - \vec{k'}) \frac{\Delta(\vec{k'})}{2E_{\vec{k'}}} \tanh \frac{\beta E_{\vec{k'}}}{2} \tag{3.63}$$

Take $\beta \to \beta_c$ gives us $E_{\vec{k'}} \to \epsilon(\vec{k'})$, and compare it with the definition of order parameter Eq.(3.46). this implies

$$\Psi(\vec{k'}) = \frac{\Delta(\vec{k'})}{2\epsilon(\vec{k'})} \tanh \frac{\beta_c \epsilon(\vec{k'})}{2} \tag{3.64}$$

Bring the above into the Eq.(3.62), gives us the final expression of Ginzburg-Landau free energy's first derivative with respect to $\Delta^\dagger(\vec{k})$:

$$\frac{\partial F_{_{CN}}}{\partial \Delta^\dagger(\vec{k})} = -\frac{1}{2}\sum_{n,\vec{k}} \Delta(\vec{k})\left(\frac{1}{E(\vec{k})}\tanh\frac{\beta E(\vec{k})}{2} - \frac{1}{\epsilon(\vec{k})}\tanh\frac{\beta_c\epsilon(\vec{k})}{2}\right) \tag{3.65}$$

We find that Eq.(3.65) is very similar to Eq.(2.13), except that Δ in Eq.(2.13) is a momentum independent order parameter, while it is not true for the Coulomb interaction's inter-nodal case. Nevertheless, we can still borrow the Taylor expansion procedure following Eq.(2.13), which yields the Ginzburg-Landau free energy's power series with respect to the order parameter $\Delta(\vec{k})$:

$$\begin{aligned}\frac{\partial F_{_{CN}}}{\partial \Delta^\dagger(\vec{k})} = \sum_{n,\vec{k}} \Delta(\vec{k})\Bigg[&\frac{f(\beta\epsilon(\vec{k})) - f(\beta_c\epsilon(\vec{k}))}{\epsilon(\vec{k})} \\ &-\left(\frac{\beta\epsilon(\vec{k})}{2} - \frac{\beta\epsilon(\vec{k})}{2}\tanh^2\frac{\beta\epsilon(\vec{k})}{2} - \tanh\frac{\beta\epsilon(\vec{k})}{2}\right)\frac{|\Delta(\vec{k})|^2}{4\epsilon(\vec{k})^3} + \cdots\Bigg]\end{aligned} \tag{3.66}$$

Integrating we get

$$\begin{aligned}F_{_{CN}} = \sum_{n,\vec{k}} \Bigg[&\frac{f(\beta\epsilon(\vec{k})) - f(\beta_c\epsilon(\vec{k}))}{\epsilon(\vec{k})}|\Delta(\vec{k})|^2 \\ &-\left(\frac{\beta\epsilon(\vec{k})}{2} - \frac{\beta\epsilon(\vec{k})}{2}\tanh^2\frac{\beta\epsilon(\vec{k})}{2} - \tanh\frac{\beta\epsilon(\vec{k})}{2}\right)\frac{|\Delta(\vec{k})|^4}{8\epsilon(\vec{k})^3} + \cdots\Bigg]\end{aligned} \tag{3.67}$$

For $T \simeq T_c$, the free energy formula reads:

$$F_{CN} = -a|\Delta|^2 + \frac{b}{2}|\Delta|^4 + \cdots \tag{3.68}$$

After comparison of these two above, we are left with the coefficients of Charge Density Wave phase in Coulomb interaction's inter-nodal case:

$$\begin{aligned}a =& \frac{4\pi}{3k_BT}\left(\frac{1}{\beta_c\hbar v}\right)^3\left(1 - \frac{T}{T_c}\right) \\ b \simeq& \frac{8\pi}{15(\hbar v)^3}\left[\frac{\ln 2}{2}\beta_c\Lambda + \frac{1}{4}\ln\left(\frac{\beta_c\Lambda}{2\pi}\right) - \frac{1}{4}\Psi\left(\frac{1}{2}\right)\right]\end{aligned} \tag{3.69}$$

Here the coefficient a is to the leading order in $(\beta_c\Lambda)^{-1}$ and $\Psi(x)$ is the digamma function.

Chapter 4

Odd Parity Superconductivity in Weyl Semi-Metals

So far, we have focused our interest on the nature of correlated phases in Weyl semi-metal systems due to repulsive interactions. We have shown that for chemical potential at the Weyl nodes, perfect nesting would lead to various particle-hole instabilities. Specifically, for local repulsive interaction, an excitonic ferromagnetic insulator state is stabilized[49]; while for attractive interactions, a Charge Density Wave[30] is realized. Here we turn to the possible instabilities due to attractive interactions. Meng and Burkov[31] studied the nature of superconducting state obtained in systems, where the superconductivity is externally induced by proximity effect. This is achieved by replacing the normal insulator by a superconductor in the Topological-Normal insulator heterostructure. They find a variety of gapless and/or topological superconducting phases which may host Majorana bound states on the surface or vortex cores. Gil Young et al.[32] studied the intrinsic superconducting instabilities of doped Weyl semimetals within a model that has C_{4h} point

group symmetry. They find that the even parity fully gapped finite momentum pairing state is energetically favored.

The point group symmetry imposed above is not necessary for Weyl semimetals. In this chapter we relax this constraint and explore the possible superconducting phases. For local attractive interactions we find the finite momentum pairing to be the ground state, while for long range interactions, a gapped BCS state would appear as a competing phase, with details of the interaction favoring one over the other. Crucially, in contrast to Gil et al. [32] we find that a "spin singlet" has no weight and that only p-wave "spin triplet" phases are allowed. The difference originates from the properties of the model under inversion. In our case the spin at momentum $\vec{k}$ and momentum $-\vec{k}$ are the same as required by inversion symmetry. On the other hand, even for inversion symmetric models, the effective low energy theory can be one where the spins are not parallel at momenta related by inversion[4]. In the latter case, singlet pairing has finite overlap with the chiral state. For the class of Weyl semi-metals studied here, we generically find odd parity superconductivity which are analogs of the ^{3}He A phase. They add to a class of spin triplet superconducting phases that display Weyl behavior [50, 51]

The approach we will take in the following is the same as the one that we used to explore excitonic phases[49]. In this regard the work is complementary to that of Gil Young et al.[32], who look at mean field decomposition in the spin basis prior to projecting to the low energy sector. We first project to the linearly dispersing chiral basis and than perform the mean field analysis. To highlight the physics, we simplify to the case of two Weyl nodes and local density density interactions. There are two types of particle-particle instabilities that can arise in this case i) intra-nodal (occurring at zero momentum) and

ii) inter-nodal (occurring at a finite fixed momentum associated with the nesting vector). The former leads to finite momentum pairing (analogous to FFLO[52, 53]) while the latter is the zero momentum pairing BCS[54] state. For local interaction, the most favorable superconducting state is the finite momentum paired odd parity axial phase. A minimum interaction strength is required to nucleate them for chemical potential at the node which is the consequence of the vanishing density of states. We also find that it is energetically less optimal than a fully gapped Charge Density Wave phase. For finite chemical potential the particle hole nesting is lost, and the axial superconductor is realized. For long range attraction a fully gapped BCS state is stabilized for all values of the chemical potential.

4.1 Model Hamiltonian

We will also start from the clean limit Hamiltonian, which gives the linearly dispersion relation between momentum and energy. Consider a system with two Weyl nodes at $\vec{K}_0 = K_0\hat{x}$ (labeled R) and $-\vec{K}_0 = -K_0\hat{x}$ (labeled L) with chiralities $+1$ and -1 respectively. The Hamiltonian is

$$H_{0\pm} = \pm\hbar v \sum_{\vec{k}} \psi^{\dagger}_{\vec{k}\alpha}\, \vec{\sigma}_{\alpha\beta} \cdot \left(\vec{k} \mp \vec{K}_0\right) \psi_{\vec{k}\beta}, \tag{4.1}$$

where v is the Fermi velocity and $\vec{\sigma} = \{\sigma_x, \sigma_y, \sigma_z\}$ is a vector of Pauli matrices. The dispersion at each node is $\epsilon_{\vec{q}} = \pm\hbar v\,|\vec{q}|$ centered around $\pm\vec{K}_0$, with $\vec{q} = \vec{k} \mp \vec{K}_0$ is the shortened form of the momentum vector. The conduction (valence) band at the R node has its spin parallel (anti-parallel) to $\vec{q}$, while the opposite is true at the L node. The general

particle-particle interaction, in momentum space, still takes the form:

$$V = \sum_{\sigma,\sigma'} \sum_{\vec{k},\vec{k}',\vec{q}} V(\vec{q}) \psi^{\dagger}_{\vec{k}'+\vec{q},\sigma'} \psi_{\vec{k}',\sigma'} \psi^{\dagger}_{\vec{k}-\vec{q},\sigma} \psi_{\vec{k},\sigma} \tag{4.2}$$

Here the upper cutoff of the momentum magnitude in integral $\Lambda/\hbar v$ is also involved, since the Weyl physics is the low energy description of a more general theory, thus this enforcement in the vicinity of Weyl points is necessary.

4.2 Particle-Hole Instabilities within Mean Field

We rewrite the interaction in the basis of the non-interacting bands. To do so we define a rotation matrix $M^{R,L}(\vec{k})_{n\sigma}$ such that $c^{L,R}_{\vec{k}n} = M^{L,R}(\vec{k})_{n\sigma} \psi^{R,L}_{\vec{k}\sigma}$. Note that the spin degeneracy is lifted and the noninteracting eigenstates are labels by $n = \pm$. The rotation matrices are unitary and rotate the spin quantization axis of each electron to point along its momentum $\vec{k}$.

We split the sum over momentum over $\vec{k}$ for each $\psi_{\vec{k},\sigma}$ into two, one with small momenta near the left node and the other with small momenta about the right node. An upper cutoff in energy, Λ, is imposed as the linear dispersion is a low energy phenomena. Of the 16 possible terms from Eq.(4.2) only 6 terms satisfy momentum conservation for scattering restricted to the states within the cutoff around the node. For every momentum $\vec{q} = q\hat{q}$, where $\hat{q} = \{\hat{q}_x, \hat{q}_y, \hat{q}_z\}$ is the unit vector along $\vec{q}$, we define two orthogonal vectors $\hat{e}^1_{\vec{q}} \equiv \hat{\theta}_{\vec{q}} = \{\hat{q}_x\hat{q}_z/\sqrt{\hat{q}_x^2+\hat{q}_y^2}, \hat{q}_y\hat{q}_z/\sqrt{\hat{q}_x^2+\hat{q}_y^2}, -\sqrt{\hat{q}_x^2+\hat{q}_y^2}\}$ and $\hat{e}^2_{\vec{q}} \equiv \hat{\phi}_{\vec{q}} = \{-\hat{q}_y/\sqrt{\hat{q}_x^2+\hat{q}_y^2}, \hat{q}_x/\sqrt{\hat{q}_x^2+\hat{q}_y^2}, 0\}$, such that $\hat{q}$, $\hat{e}^1_{\vec{q}}$ and $\hat{e}^2_{\vec{q}}$ form a right handed coordinate system (see Fig.2.1). The unit sphere is spanned by the vector $\hat{q}$ by two rotations, one about any axis perpendicular to $\hat{e}^2_{\vec{q}}$ and the another about $\hat{e}^2_{\vec{q}}$.

Construction above holds for an arbitrary quantization axis $\hat{n}$, with the corre-

sponding polar and azimuthal angle for $\vec{q}$ defined in the coordinate frame $\{\hat{l}, \hat{m}, \hat{n}\}$. In the rest of the letter we use the $\{\hat{x}, \hat{y}, \hat{z}\}$ coordinate system. The particular choice of the coordinate system breaks spatial rotational invariance.

Specializing to potentials that are even functions of $\vec{k}$, i.e. $V(\vec{k}) = V(-\vec{k})$, the interaction is

$$V_c = \sum_{\vec{k},\vec{k}',\tau,n} \Bigg[\Big(V(\vec{k}-\vec{k}') - V(\vec{k}+\vec{k}'-2\tau\vec{K}_0) \Big) \frac{\hat{e}^1_{\vec{k}} \cdot \hat{e}^1_{\vec{k}'} + \hat{e}^2_{\vec{k}} \cdot \hat{e}^2_{\vec{k}'}}{2} c^{\tau\dagger}_{\vec{k}n} c^{-\tau\dagger}_{-\vec{k}n} c^{-\tau}_{-\vec{k}'n} c^{\tau}_{\vec{k}'n} + V(\vec{k}-\vec{k}') \frac{1+\hat{k}\cdot\hat{k}'}{2} c^{\tau\dagger}_{\vec{k}n} c^{\tau\dagger}_{-\vec{k}n} c^{\tau}_{-\vec{k}'n} c^{\tau}_{\vec{k}'n} \Bigg] \tag{4.3}$$

$\tau = \pm$ refer to the two nodes. The advantage of this representation, instead of the polar and azimuthal angles, is that it allows us to avoid the double-valued nature of the spin rotation group. We have dropped terms of the form $c^{\tau_1\dagger}_{n\vec{k}} c^{\tau_2\dagger}_{-n-\vec{k}} c^{\tau_2}_{-n-\vec{k}'} c^{\tau_1}_{n\vec{k}'}$ and $c^{\tau_1\dagger}_{n\vec{k}} c^{\tau_2\dagger}_{n-\vec{k}} c^{\tau_2}_{-n\vec{k}'} c^{\tau_1}_{-n-\vec{k}'}$ which lead to pairing of states which are not degenerate in the noninteracting limit. For attractive interaction we get the very rich structure, with a number of possible superconducting phases. The first two terms in Eq.(4.3) lead to inter nodal pairing, which give the zero momentum BCS[54] state, while last term yields finite momentum pairing states (FFLO[52, 53]). In the rest of the paper we analyze the instabilities within mean field.

4.2.1 Local Interactions

For local interactions, the BCS channel vanishes. To understand why, note that the interaction is one where we destroy particles at $\vec{k}$ and $-\vec{k}$ and create them at $\vec{k}'$ and $-\vec{k}'$. Thus there are two possibilities: put the first particle at $\vec{k}'$ and the second at $-\vec{k}'$ or vice verse. These are inequivalent processes, as evident from the different momentum transfer involved, among indistinguishable particles. The exchange produces a relative minus sign.

For local interaction the weight of both the processes are identical leading to an exact cancelation. This is very different from that of the model with lower symmetry such as the C_{4h} symmetric model studied by Gil Young et al.[32], where the BCS channel is also unstable for local attraction. The reason for the difference arises from the fact that in our model the spins at $\vec{k}$ and $-\vec{k}$ are parallel for all $\vec{k}$. Thus the two process only pick up a relative sign independent of the spin orientation. For the C_{4h} symmetric models, whether the particle at $\vec{k}$ ends up at $\vec{k}'$ or $-\vec{k}'$ also determines a relative factor that accounts for the different spin orientation of the two final states. This mitigates the cancelation for all momenta. Nevertheless, in both cases the finite momentum pairing wins out. Tipping the system to favor the BCS state requires fine tuning.

In the finite momentum pairing channel, there are two equally attractive channels corresponding to order parameters of the form $\Delta_s = \left\langle \sum_{\vec{k}} c^{\tau}_{-\vec{k}n} c^{\tau}_{\vec{k}n} \right\rangle$ and $\vec{\Delta}_p = \left\langle \sum_{\vec{k}} \hat{k} c^{\tau}_{-\vec{k}n} c^{\tau}_{\vec{k}n} \right\rangle$. The former is the even parity (s-wave) while the latter is odd parity (p-wave) superconductor. Note that the anti commutation of fermionic operators implies that $\Delta_s = 0$. This is expected as non-degenerate states cannot pair in the singlet channel and only odd orbital pairing survives. For local attractive interaction, $V(\vec{k}) = g/\Omega$ where g is a constant and Ω is the volume of the system. The gap equation for the p-wave channel at zero temperature is

$$1 = \frac{g}{2} \sum_{k} \frac{\left| \hat{\Delta}_p \cdot \hat{k} \right|^2}{\sqrt{(\hbar v k)^2 + \left| \vec{\Delta}_p \cdot \hat{k} \right|^2}} \tag{4.4}$$

In general the complex order parameter takes the form $\vec{d}_1 + i\vec{d}_2$ and extremalization yields two possible structure: (i) $\vec{d}_1 \cdot \vec{d}_2 = 0$, $|\vec{d}_1| = |\vec{d}_2|$ and (ii) $\vec{d}_1 || \vec{d}_2$, $\vec{d}_1 + i\vec{d}_2 = \vec{d}e^{i\phi}$ where $\vec{d}$ is a real vector[27]. Minimization of the gap equation for the two cases yields the axial vacuum (case (i)) as the ground state and thus a chiral superconductor is stabilized. This states

has nodes in the gap, with linearly dispersing massless charged excitations, in complete analogy with the A phase of liquid ^{3}He. Equation (4.4) is identical to the gap equation obtained for the excitonic phases for repulsive interaction [49]. Reading off the results we note that a minimum interaction strength of $g_c = 3(\hbar v)^3/2\pi\Gamma^2$ is required for the state to be realized for chemical potential at the node. Here $\Gamma < \Lambda$ is the cutoff in energy of the attractive interaction. At mean field level, the Charge Density Wave instability is also possible for attractive interaction [49, 30]. The critical coupling is smaller as compared to the superconducting state and opens a full gap (i.e. no nodes). Thus the nodal finite momentum superconducting state is always disfavored as compared to the Charge Density Wave states.

At finite chemical potential the particle hole nesting between the nodes is lost and only the superconducting state is realized. Moreover, for finite chemical potential, μ, the state is precipitated for infinitesimal interaction strength. For $\mu - \Gamma > 0$ and $\mu + \Gamma < \Lambda$, the attractive interaction is operative only for the positive energy sector of the theory with linear dispersion. For this case the transition temperature is $2K_BT_c \approx \Gamma \exp[-3/g\nu(\mu)]$ where $\nu(\mu) = \mu^2/2\pi^2(\hbar v)^3$ is the density of states at the chemical potential.

4.2.2 Long-range Interactions

For local interaction $V(\vec{k} - \vec{k}') = V(\vec{k} + \vec{k}' - 2\tau\vec{K}_0)$ and no inter nodal pairing is allowed. For long range interaction, the cancelation does not occur and a BCS state can precipitate. This state competes with the intra-nodal pairing state. Which of the two wins depends on the details of the interaction. To identify the possible phases, we assume an attractive interaction of the form

$$V(\vec{k}) = \begin{cases} -g & \text{if } |\vec{k}| < |\vec{K}| < |\vec{K}_0| \\ 0 & \text{otherwise} \end{cases} \tag{4.5}$$

for some fixed $\vec{K}$. Thus the attraction has a range of order $1/|\vec{K}|$ smaller the $1/|\vec{K}_0|$. While this simplifies the algebra, the symmetry arguments below hold in general. Let us now consider the two attractive channels: (1) $\vec{\Delta}_1 = \left\langle \sum_{\vec{k}} \hat{e}^1_{\hat{k}} c^\tau_{-\vec{k}n} c^\tau_{\vec{k}n} \right\rangle$ and (2) $\vec{\Delta}_2 = \left\langle \sum_{\vec{k}} \hat{e}^2_{\hat{k}} c^\tau_{-\vec{k}n} c^\tau_{\vec{k}n} \right\rangle$. Since $\hat{e}^1_{\vec{k}}$ is even under inversion , i.e. $\hat{e}^1_{\vec{k}} = \hat{e}^1_{-\vec{k}}$, $\vec{\Delta}_1 = 0$. This is analogous to the even orbital parity channel vanishing in the intra-nodal case.

There are two possible superconducting states: (1) $\vec{\Delta}_2 = \left\langle \sum_{\vec{k}} \hat{e}^2_{\hat{k}} c^\tau_{-\vec{k}n} c^\tau_{\vec{k}n} \right\rangle = \Delta_{2p}\hat{x}$ and $\vec{\Delta}_2 = \left\langle \sum_{\vec{k}} \hat{e}^2_{\hat{k}} c^\tau_{-\vec{k}n} c^\tau_{\vec{k}n} \right\rangle = \Delta_{2c}(\hat{x} + i\hat{y})/\sqrt{2}$. The p and c label refer to polar and chiral respectively. The structure of the order parameters is dictated by symmetry. Once the spatial rotational symmetry is broken by a choice for the quantization axis, the vector $\hat{e}_2$ lies in the plane perpendicular to it. As the vector $\hat{k}$ sweeps out the unit sphere, $\hat{e}_2$ spans a unit circle in this plans (see Fig.2.1). Thus the order parameter in this case is either a polar vector in the plane (chosen to be $\hat{x}$ for illustrative purposes) or chiral. Within mean field, the spectrum for the quasi-particles for the two cases are $E_{2p} = \sqrt{(\hbar v k)^2 + |\Delta_{2s}|^2 \cos^2\phi}$ and $E_{2p} = \sqrt{(\hbar v k)^2 + |\Delta_{2c}|^2}$, where ϕ is the azimuthal angle in the $\{\hat{x}, \hat{y}, \hat{z}\}$ coordinate system. The polar state has line nodes while the chiral state is gapped. On minimization of the free energy, the latter is energetically favored. It also more favorable as compared to the finite momentum pairing state.

For chemical potential at the node a minimum coupling strength of $g_c = (\hbar v)^3/2\pi\Gamma^2$ is needed to nucleate this state. Here $\Gamma = \hbar v|\vec{K}|$ is the energy corresponding to the cut off in momentum in Eq.(4.5). Since the intra-nodal pairing depends only on the small wavelength part of the interaction, the instability criterion is the same for the interaction

in Eq.(4.5) as the short-range interaction. Since the critical coupling is three times larger in the latter case, we conclude that for long range interactions the chiral BCS state is the preferred ground state.

For finite chemical potential, the transition temperature for the chiral BCS state is $2K_BT_c \approx \Gamma \exp[-1/2g\nu(\mu)]$. Thus the transition temperature is lower than that of the finite pairing state given by $2K_BT_c \approx \Gamma \exp[-3/g\nu(\mu)]$. The difference arises from the angular dependence of the gap in the finite momentum state which has nodes at the poles.

4.3 Topological Excitations

For short range interactions the lowest energy state is the finite momentum pairing in odd parity channel. Such a state has nodes at the north and south pole of the spherical fermi surface. In complete analogy with the corresponding states for spinless version of the equal spin pairing states in ^{3}He[27], they support relativistic massless fermionic excitations. The existence of these nodal points leads to surface states at zero energy. As discussed in references [32, 55] the vortex of finite momentum pairing state is made up of two half quantum vortices, where the phase only winds around one of the Weyl nodes but not the other. The fact that Fermi surface encloses a Berry phase of π, implies that each half vortex hosts a Majorana mode at its core. In general the hybridization between the two will gap them out as they are not protected by any symmetry. For long range interaction, the odd parity BCS state wins out. This state is fully gapped.

4.4 Effect of Disorder

It is known that spin orbit interaction leads to suppression of the deleterious effects of disorder induced pair breaking on superconductivity[56]. In particular scalar disorder cannot mix states with different chirality. Stated differently scattering between different spin-momentum locked states acquire angular dependence arising from mismatch in spin orientation. The nontrivial dependence leads to vanishing dephasing rate yielding robust superconductivity[56].

4.5 Discussion

In this section we compare and contrast our work to those in the literature. To understand why only odd pairing superconductivity is obtained, it is important to note that the bands that touch are spin non degenerate. In other words, in the low energy effective theory there are two state per momentum which are split in energy. Chirality is a good quantum number but not spin. Given this, it is not possible to form spin singlets among degenerate states, as only one of the one "spin" state per momenta is available. Previous studies on the interplay of spin orbit and superconductivity [32, 31] perform a the mean field decomposition before projecting to the chiral basis. In other words a projection to singlet states is made before accounting for the splitting due to spin orbit. This allows for finite pairing amplitude among states that are non degenerate in energy in the noninteracting limit (i.e. mixes the valence and conduction bands). Fore chemical potential at the node these yield a class of even parity superconducting states for the C_{4h} symmetric models. They are absent in the class of Weyl semi-metals studied here.

Another important distinction is that in the minimal model assumed here of

two Weyl nodes, the Pauli matrices represent spin. In particular they do not change under inversion. In certain class of effective theories, inversion operator takes the form $I : \sigma^z H(-\vec{k})\sigma^z$[4, 32]. In this case the sign of the spin operators for the transverse directions changes under inversion. This additional symmetry leads to a set of superconducting states that allow for even parity spin singlet pairing. The reason is that the spin state at $\vec{k}$ and $-\vec{k}$ are no longer the same, as one would expect if inversion was an identity operator on spins. Thus there is a finite projection of singlet states onto the spin texture in the chiral basis.

A final point to note is that a full lattice model (as opposed to the low energy effective theory considered here) has linear dispersion for a finite energy window around the node. Thus any analysis that uses the full energy dispersion includes of the deviation from linearity. This is especially true for doped systems with large chemical potentials. Nevertheless the non-degeneracy of the bands and the spin structure allow for odd parity superconductors. Whether the even or odd parity states win out in this case is deferred to future investigations.

In summary Weyl semi-metals are shown to display robust odd parity superconductivity, with both zero and finite momentum cooper pairs.

Chapter 5

Conclusions

In this chapter, we present the primary conclusions of the work we done in the whole thesis.

In chapter 2, we presented the following conclusion for short-range interactions:

1. Strong spin-orbit coupling and repulsive interaction leads to novel excitonic phases in Weyl semi-metals.

2. For short-range interaction, eight novel phases are yielded, and all of them require minimum interaction strengths to ensure each phase be promoted.

3. Among all the phases yielded by the interplay between interaction and topology, a novel chiral excitonic insulator phase is of great importance, because this state, characterized by a complex vectorial order parameter, can lead to a meaningful bandgap out of the Weyl nodes.

4. The most striking feature we achieved is that the novel state, chiral excitonic phase is ferromagnetic, with the phase of the order parameter determining the direction of

the induced net spin polarization, which can serve as the experimental identification for the chiral excitonic insulator phase.

5. For the two Charge Density Wave phases promoted by the inter-nodal part of interaction, we also tried the Ginzburg-Landau free energy analysis to check whether the conclusion we get from mean-field analysis is correct. Finally, the ensurance is achieved.

For the other limit of interaction, long-range case, which is discussed in detail in chapter 3, the conclusion that we achieved are the follows:

1. Strong spin-orbit coupling and repulsive long-range interaction can also lead to novel excitonic phases in Weyl semi-metals.

2. Similar to the short-range case limit, long-range case would also yield Charge Density Wave phase from inter-nodal part of interaction, and Excitonic Insulator phase from intra-nodal part of interaction.

3. Considering the complexity of calculation with Coulomb form interaction, we only keep the leading terms for inter-nodal and intra-nodal parts. In each part, we derive the minimum interaction strength needed for the existence of each novel phase. For Charge Density Wave phase corresponding to inter-nodal part, the minimum interaction strength is $g > 2\pi^2\hbar v$; while for Excitonic Insulator phase corresponding to intra-nodal part, the minimum interaction strength reads $g > 4\pi^2\hbar v$. Therefore, under the Coulomb interaction, the most energy favorable state would be the Charge Density Wave phase, which gives the lowest value among all the interaction's minimum strengths.

Following the procedure of searching novel phases promoted by interaction-hole instabilities in Weyl semi-metal systems in chapter 2 and chapter 3, we convert to the realization of any possible superconducting states of matter in Weyl semi-metal systems in chapter 4. The following conclusion are reached there under this topic:

1. We achieved the realization of superconducting states of matter in Weyl semi-metal systems in the presence of strong spin orbit coupling.

2. As the energy spectrum has nodes at an even number of points in the Brillouin zone, consequently both intra-nodal finite momentum pairing and inter-nodal BCS superconductivity are allowed.

3. we displayed the robust odd parity superconductivity, with both zero and finite momentum cooper pairs and reached a particular case where non degenerate bands indeed can support the odd parity superconductivity with rich topological content.

4. For local attractive interaction the finite momentum pairing state with chiral p-wave symmetry is found to be most favorable at finite chemical potential. The state is an analog of the superfluid ^{3}He A phase, but with cooper pairs having finite center of mass momentum.

5. For chemical potential at the node the state is preempted by a fully gapped Charge Density Wave phase. For long-range attractive interactions, the BCS state wins out for all values of the chemical potential.

6. Finally, we compared of our work with those in literature and try to explain why only odd pairing superconductivity is obtained.

Bibliography

[1] C. W. J. Beenakker. *Colloquium*: Andreev reflection and klein tunneling in graphene. *Rev. Mod. Phys.*, 80:1337–1354, Oct 2008.

[2] D. J. Miller. Relativistic quantum mechanics. SUPA Graduate School, Oct 2008.

[3] Xiangang Wan, Ari M. Turner, Ashvin Vishwanath, and Sergey Y. Savrasov. Topological semimetal and fermi-arc surface states in the electronic structure of pyrochlore iridates. *Phys. Rev. B*, 83:205101, May 2011.

[4] A. A. Burkov and Leon Balents. Weyl semimetal in a topological insulator multilayer. *Phys. Rev. Lett.*, 107:127205, Sep 2011.

[5] Jeffrey C. Y. Teo, Liang Fu, and C. L. Kane. Surface states and topological invariants in three-dimensional topological insulators: Application to $Bi_{1-x}Sb_x$. *Phys. Rev. B*, 78:045426, Jul 2008.

[6] Liang Fu, C. L. Kane, and E. J. Mele. Topological insulators in three dimensions. *Phys. Rev. Lett.*, 98:106803, Mar 2007.

[7] Rahul Roy. Topological phases and the quantum spin hall effect in three dimensions. *Phys. Rev. B*, 79:195322, May 2009.

[8] J. E. Moore and L. Balents. Topological invariants of time-reversal-invariant band structures. *Phys. Rev. B*, 75:121306, Mar 2007.

[9] B. A. Bernevig, T. L. Hughes, and Shou-Cheng Zhang. Quantum spin hall effect and topological phase transition in hgte quantum wells. *Science*, 314:1757, Dec 2006.

[10] A. A. Zyuzin, Si Wu, and A. A. Burkov. Weyl semimetal with broken time reversal and inversion symmetries. *Phys. Rev. B*, 85:165110, Apr 2012.

[11] A. A. Zyuzin and A. A. Burkov. Topological response in weyl semimetals and the chiral anomaly. *Phys. Rev. B*, 86:115133, Sep 2012.

[12] Jian-Hua Jiang. Tunable topological weyl semimetal from simple-cubic lattices with staggered fluxes. *Phys. Rev. A*, 85:033640, Mar 2012.

[13] K. S. Novoselov, A. K. Geim, S. V. Morozov, D. Jiang, Y. Zhang, S. V. Dubonos, I. V. Grigorieva, and A. A. Firsov. Electric field effect in atomically thin carbon films. *Science*, 306:666–669, Oct 2004.

[14] A. H. Castro Neto, F. Guinea, N. M. R. Peres, K. S. Novoselov, and A. K. Geim. The electronic properties of graphene. *Rev. Mod. Phys.*, 81:109–162, Jan 2009.

[15] M. Z. Hasan and C. L. Kane. *Colloquium*: Topological insulators. *Rev. Mod. Phys.*, 82:3045–3067, Nov 2010.

[16] Xiao-Liang Qi and Shou-Cheng Zhang. Topological insulators and superconductors. *Rev. Mod. Phys.*, 83:1057–1110, Oct 2011.

[17] Castro Neto, A. H., F. Guinea, and N. M. R. Peres. *Phys. World*, 19:33, 2006.

[18] M. I. Katsnelson, K. S. Novoselov, and A. K. Geim. *Nat. Phys.*, 2:620, 2006.

[19] M. I. Katsnelson and K. S. Novoselov. *Solid State Commun.*, 143:3, 2007.

[20] C. L. Kane and E. J. Mele. Quantum spin hall effect in graphene. *Phys. Rev. Lett.*, 95:226801, Nov 2005.

[21] C. L. Kane and E. J. Mele. Z_2 topological order and the quantum spin hall effect. *Phys. Rev. Lett.*, 95:146802, Sep 2005.

[22] Congjun Wu, B. Andrei Bernevig, and Shou-Cheng Zhang. Helical liquid and the edge of quantum spin hall systems. *Phys. Rev. Lett.*, 96:106401, Mar 2006.

[23] E. Abers. *Quantum Mechanics*. Pearson Ed., Addison Wesley, Prentice Hall Inc.,, 2004.

[24] G Woan. *The Cambridge Handbook of Physics Formulas*. Cambridge University Press, 2010.

[25] Hermann Weyl. Gravitation and the electron. *Proc.Nat.Acad.Sci.15.323*, 15:323, Mar 1929.

[26] Conyers Herring. Accidental degeneracy in the energy bands of crystals. *Phys. Rev.*, 52:365–373, Aug 1937.

[27] G. E. Volovik. *Universe in a Helium Droplet*. Oxford University Press, 2003.

[28] T. Tsuneto. *Supercondutivity and Superfluidity*. Cambridge University Press, 1998.

[29] Huazhou Wei, Sung-Po Chao, and Vivek Aji. Odd parity superconductivity in weyl semimetals. *arXiv:1305.7233*, May 2013.

[30] Zhong Wang and Shou-Cheng Zhang. Chiral anomaly, charge density waves, and axion strings from weyl semimetals. *Phys. Rev. B*, 87:161107, Apr 2013.

[31] Tobias Meng and Leon Balents. Weyl superconductors. *Phys. Rev. B*, 86:054504, Aug 2012.

[32] Gil Young Cho, Jens H. Bardarson, Yuan-Ming Lu, and Joel E. Moore. Superconductivity of doped weyl semimetals: Finite-momentum pairing and electronic analog of the ^{3}He-A phase. *Phys. Rev. B*, 86:214514, Dec 2012.

[33] C. Kallin and A. J. Berlinsky. Is Sr_2RuO_4 a chiral p-wave superconductor? *J. Phys. Condens. Matter*, 21:164210, 2009.

[34] Kai-Yu Yang, Yuan-Ming Lu, and Ying Ran. Quantum hall effects in a weyl semimetal: Possible application in pyrochlore iridates. *Phys. Rev. B*, 84:075129, Aug 2011.

[35] Vivek Aji. Adler-bell-jackiw anomaly in weyl semimetals: Application to pyrochlore iridates. *Phys. Rev. B*, 85:241101, Jun 2012.

[36] M. A. Subramanian, G. Aravamudan, and G. V. Subba Rao. Oxide pyrochlores - a review. *Prog. Solid St. Chem*, 15:55–143, 1983.

[37] Steven T. Bramwell and Michel J. P. Gingras. Spin ice state in frustrated magnetic pyrochlore materials. *Science*, 294:1495–1501, Nov 2001.

[38] Jason S. Gardner, Michel J. P. Gingras, and John E. Greedan. Magnetic pyrochlore oxides. *Rev. Mod. Phys.*, 82:53–107, Jan 2010.

[39] N. Taira, M. Wakeshima, and Y. Hinatsu. Magnetic properties of iridium pyrochlores $R_2Ir_2O_7$ (R = Y, Sm, Eu and Lu). *J.Phys.Condens.Matter*, 13:5527, 2001.

[40] D. Yanagishima and Y. Maeno. Metal-nonmetal changeover in pyrochlore iridates. *J.Phys.Soc.Jpn.*, 70:2880–2883, Jun 2001.

[41] W. Kohn. Excitonic phases. *Phys. Rev. Lett.*, 19:439–442, Aug 1967.

[42] N. W. Ashcroft and N. D. Mermin. *Solid State Physics*, chapter 33, pages 715–718. Thomson Learning, Inc., 1976.

[43] V. L. Ginzburg and L. D. Landau. On the theory of superconductivity. *Zh. Eksp. Teor. Fiz.*, 20:1064, 1950.

[44] J. Sabio, F. Sols, and F. Guinea. Variational approach to the excitonic phase transition in graphene. *Phys. Rev. B*, 82:121413, Sep 2010.

[45] O. V. Gamayun, E. V. Gorbar, and V. P. Gusynin. Gap generation and semimetal-insulator phase transition in graphene. *Phys. Rev. B*, 81:075429, Feb 2010.

[46] Richard Courant and David Hilbert. *Methods of Mathematical Physics*, volume I. Wiley-Interscience, 1962.

[47] L. C. Biedenharn and J. D. Louck. *Angular Momentum in Quantum Physics*, volume 8. Addison-Wesley, Reading, 1981.

[48] Milton Abramowitz and Irene A. Stegun. *Handbook of Mathematical Functions with Formulas, Graphs, and Mathematical Tables*. New York: Dover Publications, 1970.

[49] Huazhou Wei, Sung-Po Chao, and Vivek Aji. Excitonic phases from weyl semimetals. *Phys. Rev. Lett.*, 109:196403, Nov 2012.

[50] Yi Li and Congjun Wu. the j-triplet cooper pairing with magnetic dipolar interactions. *Scientific Reports*, 2, May 2012.

[51] Jay D. Sau and Sumanta Tewari. Topologically protected surface majorana arcs and bulk weyl fermions in ferromagnetic superconductors. *Phys. Rev. B*, 86:104509, Sep 2012.

[52] Peter Fulde and Richard A. Ferrell. Superconductivity in a strong spin-exchange field. *Phys. Rev.*, 135:A550–A563, Aug 1964.

[53] A. I. Larkin and Yu. N. Ovchinnikov. Nonuniform state of superconductors. *Sov. Phys. JETP*, 20, 1965.

[54] J. Bardeen, L. N. Cooper, and J. R. Schrieffer. Microscopic theory of superconductivity. *Phys. Rev.*, 106:162–164, Apr 1957.

[55] Ol'ga Dimitrova and M. V. Feigel'man. Theory of a two-dimensional superconductor with broken inversion symmetry. *Phys. Rev. B*, 76:014522, Jul 2007.

[56] Karen Michaeli and Liang Fu. Spin-orbit locking as a protection mechanism of the odd-parity superconducting state against disorder. *Phys. Rev. Lett.*, 109:187003, Oct 2012.

Appendix A

Interaction Part of Hamiltonian

In this appendix we comment on the nature of repulsive interactions. While Eq.(2.2) in the free Hamiltonian (H_0) energy spin basis $\eta^{R,L}_{\vec{q},\pm} c^{R,L}_{\vec{q},\pm}$ have a number of terms, states that conserve momentum and energies are the only ones of relevance. For completeness we show the possible terms. Here we list all interactions related to particle-hole instabilities by writing $V \simeq V_1 + V_2 + V_3 + \ldots$ with V_1 corresponds to the terms in Eq.(2.3).

$$
\begin{aligned}
V_1 = -\sum_{\vec{k},\vec{k}',n=\pm} \Bigg[& V(\vec{k}-\vec{k}') \frac{\hat{e}_{\vec{k}} \cdot \hat{e}^*_{\vec{k}'} + \hat{e}^*_{\vec{k}} \cdot \hat{e}_{\vec{k}'}}{4} \sum_{\tau=R,L} c^{\tau\dagger}_{\vec{k},n} c^{\tau}_{\vec{k},-n} c^{\tau\dagger}_{\vec{k}',-n} c^{\tau}_{\vec{k}',n} \\
& + V(\vec{k}-\vec{k}'-2\vec{K}_0) \frac{\hat{e}_{\vec{k}} \cdot \hat{e}_{\vec{k}'} + \hat{e}^*_{\vec{k}} \cdot \hat{e}^*_{\vec{k}'}}{2} c^{L\dagger}_{\vec{k},n} c^{L}_{\vec{k},-n} c^{R\dagger}_{\vec{k}',-n} c^{R}_{\vec{k}',n} \\
& - \Big[2V(2\vec{K}_0) - V(\vec{k}-\vec{k}') \Big(1 + \hat{k} \cdot \hat{k}' \Big) \Big] c^{L\dagger}_{\vec{k},n} c^{R}_{\vec{k},-n} c^{R\dagger}_{\vec{k}',-n} c^{L}_{\vec{k}',n} \Bigg] \\
V_2 = -\sum_{\vec{k},\vec{k}',n=\pm} \Bigg[& V(\vec{k}-\vec{k}') \frac{\hat{e}_{\vec{k}} \cdot \hat{e}_{\vec{k}'} + \hat{e}^*_{\vec{k}} \cdot \hat{e}^*_{\vec{k}'}}{4} \sum_{\tau=R,L} c^{\tau\dagger}_{\vec{k},n} c^{\tau}_{\vec{k},-n} c^{\tau\dagger}_{\vec{k}',n} c^{\tau}_{\vec{k}',-n} \\
& + V(\vec{k}-\vec{k}'-2\vec{K}_0) \frac{\hat{e}_{\vec{k}} \cdot \hat{e}_{\vec{k}'} + \hat{e}^*_{\vec{k}} \cdot \hat{e}^*_{\vec{k}'}}{2} c^{L\dagger}_{\vec{k},n} c^{L}_{\vec{k},-n} c^{R\dagger}_{\vec{k}',n} c^{R}_{\vec{k}',-n} \\
& - \Big[2V(2\vec{K}_0) - V(\vec{k}-\vec{k}') \Big(1 - \hat{k} \cdot \hat{k}' \Big) \Big] c^{L\dagger}_{\vec{k},n} c^{R}_{\vec{k},-n} c^{R\dagger}_{\vec{k}',n} c^{L}_{\vec{k}',-n} \Bigg]
\end{aligned}
\tag{A.1}
$$

In the above expression, we have written all the terms yielded by the particle-hole

possibilities, which are split into V_1 and V_2. Each term in V_2, represents one possible case of annihilating two particles in valance band(s) and creating them in conducting band(s), which hold(s) higher energy than valance band(s). Thus, all the terms in V_2 violate the conservation of energy. In contrast, V_1's terms are allowed from energy perspective and retained in chapters 2 and 3 (Eq.(2.3)).

Appendix B

Particle-Hole instability due to Attractive Interaction

Our work, described in chapter 2 and chapter 3 has focused on possible phase arising from repulsive interactions. In particular we find that for local interaction a ferromagnetic insulating phase is stabilized, while for long range interaction the CDW is the energetically favored phase. An intriguing possibility is that attractive local interactions can also yield a CDW phase. This was reported on in ref.[30]. For completeness we discuss the main results.

In order to understand the result, let's return to Eq.(2.3), which is used in our repulsive interaction analysis:

$$\begin{aligned} V = -\sum_{\vec{k},\vec{k}',n=\pm} \Bigg[& V(\vec{k}-\vec{k}')\frac{\hat{e}_{\vec{k}}\cdot\hat{e}^*_{\vec{k}'}+\hat{e}^*_{\vec{k}}\cdot\hat{e}_{\vec{k}'}}{4}\sum_{\tau=R,L} c^{\tau\dagger}_{\vec{k},n}c^{\tau}_{\vec{k},-n}c^{\tau\dagger}_{\vec{k}',-n}c^{\tau}_{\vec{k}',n} \\ & +V(\vec{k}-\vec{k}'-2\vec{K}_0)\frac{\hat{e}_{\vec{k}}\cdot\hat{e}_{\vec{k}'}+\hat{e}^*_{\vec{k}}\cdot\hat{e}^*_{\vec{k}'}}{2}c^{L\dagger}_{\vec{k},n}c^{L}_{\vec{k},-n}c^{R\dagger}_{\vec{k}',-n}c^{R}_{\vec{k}',n} \\ & -\Big[2V(2\vec{K}_0)-V(\vec{k}-\vec{k}')\Big(\hat{k}\cdot\hat{k}'+1\Big)\Big]c^{L\dagger}_{\vec{k},n}c^{R}_{\vec{k},-n}c^{R\dagger}_{\vec{k}',-n}c^{L}_{\vec{k}',n}\Bigg] \end{aligned} \tag{B.1}$$

Both of the two terms representing intra-nodal interaction(first two lines), cannot produce any excitonic insulator phases, due to the attractive(negative) property of $V(\vec{k})$. This conclusion is true no matter what limit $V(\vec{k})$ takes, either short-range limit(local momentum-independent form) or long-range limit(Coulomb interaction form). When $V(\vec{k})$ is long-ranged (Coulomb interaction form), $V(2\vec{K_0})$ in the third line can be neglected. This leads to the inter-nodal part interaction in the third line be positive when the potential is negative (attractive). Therefore, long-range limit of attractive $V(\vec{k})$, can not yield charge density wave phases either. So, the final possibility for charge density wave state to exist is under short-range attractive $V(\vec{k})$. This indeed is the case. While $V(\vec{k})$ is a momentum-independent negative value, notice that the last line inside the bracket is positive, while there is an overall minus sign outside. Hence the CDW phase is expected for attractive local interactions. It is important to bear in mind that attractive interactions also lead to superconducting instabilities that compete with the CDW state. In chapter 4, we explore that interplay and deal with the superconducting instabilities.